

RESEARCH ARTICLE

Grayscale Image Enhancement Using Water Cycle Algorithm

EYOB MERSHA WOLDAMANUEL 

School of Electrical and Computer Engineering, Haramaya Institute of Technology, Haramaya University, Dire Dawa, Ethiopia

e-mail: eyob.mersha12@gmail.com

ABSTRACT Recent developments in engineering and computer sciences have heightened the need for digital image enhancement. Most of the previously reported works, however, focused on image enhancement using classical methods like mathematical transformations and spatial and frequency-domain methods. Hence, recently, there has been an increasing interest in using nature-inspired optimization techniques for image processing purposes. The water cycle algorithm (WCA) is one of the nature-inspired algorithms (NIAs) that have gotten much attention in optimizing real-world engineering problems due to its appealing performance. However, to the best of the author's knowledge, little research has been undertaken on the WCA's image-enhancing capacity. Thus, this work is intended to offer a modified histogram equalization (HE) approach using WCA to enhance the contrast of an image and maintain its brightness. Besides, the proposed WCA-based image enhancement technique was compared to linear contrast stretching (LCS), HE and its modified versions, particle swarm optimization (PSO), and accelerated particle swarm optimization (APSO). In addition to the objective function fitness, 11 full reference (FR) image quality assessment (IQA) metrics were employed to evaluate image quality and compare performance. Experimental results showed that the suggested image enhancement technique exhibited better performance than others in enhancing dark grayscale images in terms of objective function fitness and perceptual visual IQA metrics like multi-scale structural similarity (MS-SSIM), information-weighted structural similarity (IW-SSIM), information-weighted mean squared error (IW-MSE), and information-weighted peak signal-to-noise ratio (IW-PSNR). The proposed method also demonstrated a faster convergence time to an optimum solution.

INDEX TERMS Grayscale image, histogram equalization, image edge detection, image enhancement, image quality assessment metrics, nature-inspired algorithms, water cycle algorithm.


I. INTRODUCTION

Image enhancement is one of the critical image-processing operations that have received considerable attention due to its usefulness in many applications [1], [2]. It is applied when a high-quality image needs to be extracted from a low-quality image input and is ready for further analysis [3], [4], [5]. It improves an image's qualities in terms of contrast, brightness characteristics, reduction of noise contents [6], etc. This can be accomplished by enlarging the intensity difference between the image part that needs to be enhanced and the background of an image. The enhancement process itself does not increase the inherent information contained

in the data. It simply emphasizes certain specified image characteristics [7].

These days, the need to have enhanced images are highly required in several disciplines, such as autonomous driving [8], [9], [10], computer vision, pattern recognition [11], face recognition [6], [12], [13], [14], [15], [16], remote sensing [17], [18], medical image analysis [19], [20], [21], [22], [23], [24], [25], animal and plant disease detection [26], [27], [28], geographical information systems (GIS), smart transportation [29], [30], and autonomous navigation [8]. Furthermore, recent developments in engineering and computer sciences have heightened the need for digital image processing.

Researchers have been implementing different mathematical algorithms and techniques to get visually appealing and

The associate editor coordinating the review of this manuscript and approving it for publication was Abdullah Ilyasu .

enhanced images [5], [31]. Although there have been dozens of techniques proposed in the field of image enhancement, many of them depend on histogram equalization (HE) [31]. Most of the research works concerning image enhancement have used classical methods like mathematical transformations, spatial domain and frequency domain methods, HE, and HE-based techniques [2], [21], [32]. In recent years, there has been a rising interest in using optimization algorithms for image processing purposes including image enhancement [3], [33], [34], [35], [36]. Among these algorithms, many researchers use fuzzy logic, neural networks [8], and nature-inspired algorithms (NIA) [3] like particle swarm optimization (PSO), accelerated particle swarm optimization (APSO), and water cycle algorithms (WCA) [32].

Bi-Histogram Fuzzy Contrast Stretching (BHFCS), a technique developed by Dhal and Das [38], has been used to improve the contrast of both grayscale and color images. The parameters of this method were optimized using a modified Chaotic Differential Evolution (CDE) with the help of Fractal Dimension (FD). Based on the intuition that image structure information is extracted from local variance distribution, the image quality index based on Local Variance (QILV) was utilized as the objective function. The augmented image's structural information is maintained when QILV rises. Therefore, the combination of FD and QILV is used as an objective function to carry out the proper enhancement. Using log transformation, Samanta et al. [39] created a technique to improve aerial photography taken by small unmanned aerial vehicles (MUAVs). Contrast and edge information make up the objective function used to assess the suggested method's image enhancement. The metaheuristic technique known as the Firefly algorithm is used to optimize the parameter that is used in the objective function. Another log transform-based technique used for improving medical images was suggested by Ashour et al. [40]. The Cuckoo Search (CS) algorithm was used in [40] to find the ideal log transformation function parameter settings.

Though WCA has been employed to optimize different constrained engineering problems, it has not been extensively utilized in image enhancement applications. To the best of the author's knowledge, there has not been much investigation conducted on the image-enhancing ability of the WCA. Of course, there are a handful of research projects that exploit the WCA for image-processing applications. This is one of the motivations for carrying out this investigation. In [41], WCA coupled with Masi Entropy (ME-WCA) is used to conduct color image segmentation. Kaushal et al. [32] use a novel HE method inspired by the principles of the WCA. This proposed method first smooths the Y channel of YCbCr color space and divides the input frame into two components using Otsu's 2D thresholding. A set of weighing constraints has been formulated and applied to both components individually in a controlled manner. The WCA has been employed to exploit an optimal value of weighing factors for the enforcement of constraints on individual components. A 3D objective

function has been designed to suitably perform an equalization and control enhancement process.

In this research work, WCA, a nature-inspired optimization algorithm, is employed along with HE to enhance grayscale images. Additionally, the performance of WCA has been compared to HE and its modified techniques, such as linear contrast stretching (LCS), contrast-limited adaptive histogram equalization (CLAHE), local contrast modification-contrast-limited adaptive histogram equalization (LCM-CLAHE), and NIAs like PSO, APSO.

The remainder of this paper is structured as follows. Section II first introduces the different image enhancement methods. A detailed discussion of the WCA follows. In this section, the proposed WCA algorithm, proposed method flow chart, and image quality assessment (IQA) metrics are extensively discussed. Section III presents the result and discussion parts of the paper. In this section, a comparative analysis of WCA-based image enhancement is made with the aforementioned techniques. Finally, Section IV concludes the research work.

The main contributions of this research work are summarized below:

- Investigate the capabilities of the WCA in image enhancement operation.
- Comparative study of this proposed algorithm (WCA) with HE and its variant image enhancement operations, PSO, and APSO.

II. METHODOLOGY

In the vast majority of image enhancement research, it is revealed that the cause of a low-quality image is low illumination at the moment of image capture [3]. Another critical cause of image quality degradation occurs when an image is converted or exported from one format to another [7]. To circumvent this problem, several researchers employ contrast enhancement as an image enhancement technique [3]. A discussion of the different traditional and optimization algorithm-based image enhancement techniques is presented in the following subsections.

A. IMAGE ENHANCEMENT TECHNIQUES

Several image enhancement techniques are available that reduce image noise, highlight edges, or show digitalized images [1]. Image enhancement algorithms are generally interactive and application-dependent [42]. The idea behind enhancement techniques is to bring out obscure details or highlight certain features of interest in an image. The most challenging task in image enhancement is measuring the criteria for enhancement. Therefore, the vast majority of image enhancement operations are empirical and required an interactive procedure to obtain a satisfactory result [37]. However, image enhancement remains a key area due to its usefulness in all image-processing applications.

1) HE AND ITS MODIFIED VERSIONS

Due to its simplicity of implementation and ease of use, HE is the most regarded and widely employed spatial gray level contrast enhancement technique [5], [7], [32], [43], [44]. It can be done by normalizing the cumulative density function (CDF) of the image, thus resulting in a uniform distribution of intensity in the image [21]. HE smooths and enlarges the dynamic range of the image histogram thereby improving the contrast of the image and giving an overall contrast enhancement. As a result, obscured details in dark areas can be made to reveal themselves, and the input image can be considerably enhanced visually [33]. On the other hand, uniform areas like smooth backgrounds lead to large peaks in the histogram, resulting in over-enhancement in the image [44]. Furthermore, HE gives priority to global enhancement over local contrast and thus ignores the local details of the image. Additional drawbacks of HE include brightness migration and artifacts [2]. HE automatically determines a transformation function that strives to equalize the histogram distribution in the output image. When an automatic enhancement is desired, this is a good method because of its predictability and ease of implementation [45], [46].

A broad discussion of the different HE-based image enhancement techniques has been found in [1], [33], and [47]. Of the available nonlinear HE transformations, CLAHE is a widely applied image enhancement technique that is best suited for dealing with 2D images. CLAHE and a modification of it have been utilized for several image enhancement applications like medical image analysis [24], underwater image enhancement [48], [49], and so on.

Contrast stretching is an image enhancement operation that makes an image look better to human perception. Its major goal is to modify the local contrast in different sections of the image so that features in dark or bright regions are brought out and displayed to human viewers [50].

CLAHE was first introduced by Ali M. Reza [33]. This algorithm successfully alleviates the block effect that arises in the enhancement process and limits local contrast enhancement by setting a threshold. This algorithm overcomes the over-enhancement problem of HE by minimizing noise-like artifacts in homogeneous regions. In CLAHE, the image is partitioned into equally-sized rectangular blocks while HE is performed in each block [51]. Based on CLAHE, many studies have been done on image contrast enhancement [24], [46], [52], [53].

LCM-CLAHE was proposed by S. Mohan and M. Ravishankar to detect breast cancer. The main reason the LCM-CLAHE came into existence was the need to overcome the over-enhancement of CLAHE, which resulted in the loss of some local information. To improve the capability of local contrast enhancement and preserve the local details in the images LCM-CLAHE utilizes two stages of image processing operations. The primary operation is local contrast enhancement and then CLAHE is applied to the local contrast-modified (LCM) image [51].

B. NIA-BASED IMAGE ENHANCEMENT

These days, due to their optimization efficiency, NIAs are applied to optimize image processing operations [54], [55] including image enhancement [56], [57]. Among these NIEs, cuckoo search is employed for gray level [58], [59] and low contrast image enhancement [60]. In [61] bat algorithm, chaotic lévy [59], and PSO combined with chaotic sequence [62] are utilized to enhance an image. Since it has offered better solutions than several optimizers [63], the WCA image enhancement efficiency was examined in this study. In addition, image enhancement utilizing PSO, APSO was performed in this study for comparison purposes.

1) PARTICLE SWARM OPTIMIZATION (PSO)

This meta-heuristic technique was developed nearly three decades ago, in 1995. It was the result of inspiration from the choreography of a bird flock and was developed by Kennedy and Eberhart [45]. The method can be thought of as a distributed behavioral algorithm that conducts a multidimensional search. Though PSO is recommended as a very efficient optimization algorithm in widespread literature, it may sometimes suffer from premature convergence for highly multimodal problems [64].

2) ACCELERATED PARTICLE SWARM OPTIMIZATION (APSO)

The particle swarm optimization uses the current global best, $gbest^t$ and the individual best, $pbest_i^t$. The objective for utilizing the individual best is to improve the diversity of quality answers; however, this diversity can be approximated by introducing some randomness into the equation. Consequently, unless there are severe non-linearity and multimodal characteristics in the problem to be solved, there is no need to utilize the individual best. A simplified version that could increase the convergence of the algorithm is to use the global best only [65]. APSO was developed by Yang in 2008 [64], [66] and then advanced further in recent studies.

3) WATER CYCLE ALGORITHM (WCA)

The WCA was developed by Hadi Eskandar, Ali Sadollah, Ardeshir Bahreininejad, and Mohd Hamdi almost a decade ago. It is the result of natural inspiration that mimics the flow of rivers and streams toward the sea and is derived from the observation of the water cycle process [63], [67].

C. WCA

1) BASIC CONCEPTS

WCA is inspired by nature, which imitates the flow of streams, and rivers down to the sea and is derived from the observation of the hydrological cycle process [64], [68].

Streams and rivers always move toward the most stable locations downhill, ending up in seas and oceans. This implies that most rivers are formed at the top of mountains and plateaus, where water is collected from rain, snow, and glacier melt. Fig.1 depicts the water cycle (hydrological cycle). In this cycle, water evaporates from water bodies, and plants

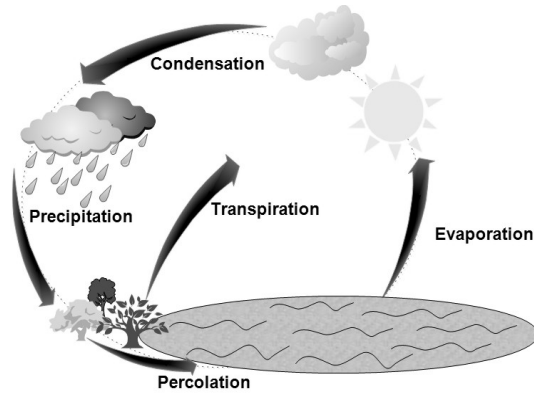


FIGURE 1. Simplified diagram of the hydrologic cycle (water cycle).

release water during photosynthesis through a process called transpiration. The evaporated and transpired water goes to the upper atmosphere, where it forms a cloud. When the atmosphere becomes colder, the cloud condenses and is poured back into the earth as rain and precipitation.

In addition to flowing to the surface, streams, rivers, snow melts, and rainfall penetrates the earth’s surface and flow similarly, downhill, beneath the earth’s surface. The aquifer that is found under the earth’s surface is sometimes called groundwater. The groundwater may join the stream, river, or lake that is found downhill (see the percolation part of Fig. 1). Besides, a considerable amount of groundwater is sucked up by greenery. This groundwater, in turn, evaporates from the lake and river and transpires from the greenery that sucked it in. This contributes to more clouds and, hence, more rain and precipitation.

2) THE PROPOSED WCA

Like other meta-heuristic algorithms, the proposed method begins with an initial population called raindrops. It is assumed that there will be rain or precipitation at the very beginning. Among the raindrops of this rain, the best individual (the best raindrop) is chosen as a sea. Then, several good raindrops are selected a river, and the rest of the raindrops are considered as streams that flow to the rivers and sea. Based on the amount of flow, each river takes water from the streams, and the amount of water entering rivers and/or the sea is different from stream to stream. Finally, rivers flow to the sea, which is the greatest downhill scene [63].

a: CREATE THE INITIAL POPULATION

It is customary practice to form an array of values for problem variables so as to solve an optimization problem employing population-based meta-heuristic methods. In WCA, a particle position is called a “Raindrop” for a single solution. When the optimization problem in question is multidimensional, then the raindrop is an array of $1 \times N_{var}$. This array is given in (1)

$$\text{Raindrop} = [x_1, x_2, x_3, \dots, x_{N-1}, x_N] \tag{1}$$

The optimization algorithms will embark on once a candidate representing a matrix of raindrops of size $N_{pop} \times N_{var}$ is generated (i.e., a population of raindrops), where N_{var} is its dimension. Thus, this matrix, which is randomly generated, is given as (rows and columns are the number of population and the number of design variables, respectively).

Population of rain drops

$$= \begin{bmatrix} \text{Raindrop}_1 \\ \text{Raindrop}_2 \\ \text{Raindrop}_3 \\ \vdots \\ \text{Raindrop}_{N_{pop}-1} \\ \text{Raindrop}_{N_{pop}} \end{bmatrix} = \begin{bmatrix} x_1^1 & x_2^1 & \dots & \dots & \dots & x_{N_{var}-1}^1 & x_{N_{var}}^1 \\ x_1^2 & x_2^2 & \dots & \dots & \dots & x_{N_{var}-1}^2 & x_{N_{var}}^2 \\ x_1^3 & x_2^3 & \dots & \dots & \dots & x_{N_{var}-1}^3 & x_{N_{var}}^3 \\ \vdots & \vdots & \dots & \dots & \dots & \vdots & \vdots \\ x_1^{N_{pop}-1} & x_2^{N_{pop}-1} & \dots & \dots & \dots & x_{N_{var}-1}^{N_{pop}-1} & x_{N_{var}}^{N_{pop}-1} \\ x_1^{N_{pop}} & x_2^{N_{pop}} & \dots & \dots & \dots & x_{N_{var}-1}^{N_{pop}} & x_{N_{var}}^{N_{pop}} \end{bmatrix} \tag{2}$$

Each of the decision variable values ($x_1, x_2, x_3, \dots, x_{N_{var}}$) can be represented as floating-point numbers (real values) or as a predefined set for continuous and discrete problems, respectively. The cost of a raindrop is obtained by the evaluation of the fitness function $F(I_E)$ given as:

$$F(I_E)_i = \text{Fitness}_i = (x_1^i, x_2^i, \dots, x_{N_{var}-1}^i \dots, x_{N_{var}}^i) \tag{3}$$

$$i = 1, 2, 3, \dots, N_{pop}$$

where N_{pop} and N_{var} are the number of raindrops (initial population) and the number of design variables, respectively. In the first step, N_{pop} raindrops or streams are created. Several N_{sr} from the best individuals (minimum values) are selected as sea and rivers. The raindrop, which has the minimum value among others, is considered a sea. In fact, N_{sr} is the summation of the Number of Rivers (a user parameter) and a single sea as given in (4). The rest of the population (raindrops form the streams that flow to the rivers or may directly flow to the sea) is calculated using (5).

$$N_{sr} = \text{Number of Rivers} + 1, \text{ where '1' stands for sea} \tag{4}$$

$$N_{\text{Raindrops}} = N_{pop} - N_{sr} \tag{5}$$

Equation (6) gives the flow intensity based on which raindrops are elected/assigned to rivers and sea.

$$NS_n = \text{round} \left[\left| \frac{\text{Fitness}_n}{\sum_{i=1}^{N_{sr}} \text{Fitness}_i} \right| \times N_{\text{Raindrops}} \right] \tag{6}$$

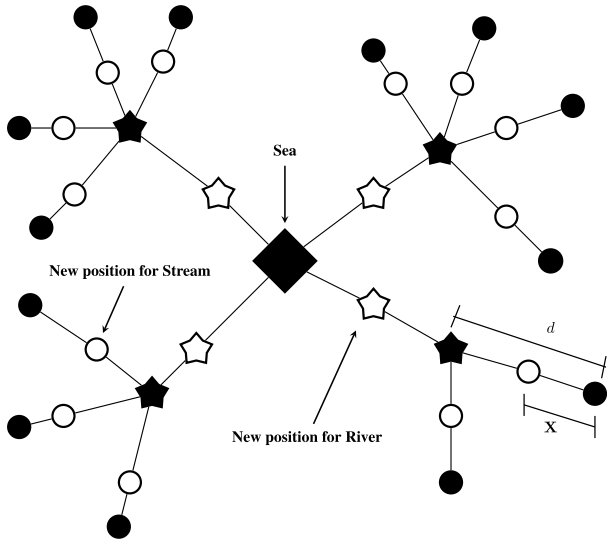


FIGURE 2. Schematic diagram of how streams flow to the rivers and also rivers flow to the sea.

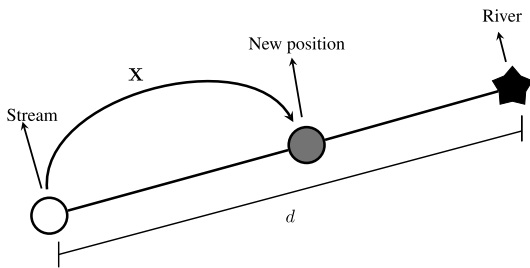


FIGURE 3. Schematic diagram of a stream flowing into river.

where NS_n is the number of streams that flow to the specific rivers or sea.

b: HOW DOES THE STREAM FLOW TO THE RIVERS OR SEA?

In this section, a mathematical description explaining how streams flow directly to the sea or to the river is presented. Fig. 3 depicts the graphical representation of the stream’s flow towards a specific river. In this figure, a stream flows to the river along the linking path between them using a randomly chosen distance given as follows:

$$X \in (0, C \times d), \quad C > 1 \tag{7}$$

Fig. 2 is a schematic diagram of how streams flow to the rivers and rivers flow to the sea. It resembles a tree or the roots of a tree.

where C is a value between 1 and 2 (near 2). $C = 2$ can be selected. The instantaneous distance between stream and river is denoted as d . In (7), X is the value that is a randomly distributed number (uniformly or maybe any appropriate distribution) between 0 and the value returned by $C \times d$. If the value of $C > 1$, it implies that streams flow in different directions toward the rivers.

This concept may also be used in describing rivers to the sea. Therefore, the new position for streams and rivers may

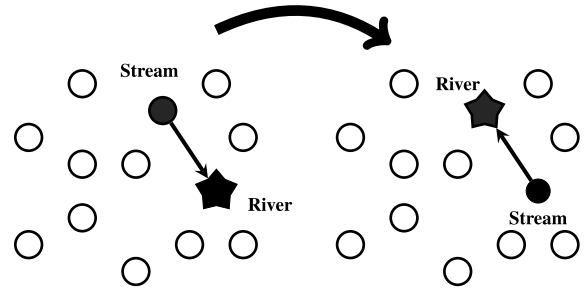


FIGURE 4. Exchanging the positions of the stream and the river where star represents river and black circle shows the best stream among other streams.

be given as

$$X_{Stream}^{(i+1)} = X_{Stream}^i + rand \times C \times (X_{River}^i - X_{Stream}^i) \tag{8}$$

$$X_{Stream}^{(i+1)} = X_{Stream}^i + rand \times C \times (X_{Sea}^i - X_{Stream}^i) \tag{9}$$

$$X_{River}^{(i+1)} = X_{River}^i + rand \times C \times (X_{Sea}^i - X_{River}^i) \tag{10}$$

where i is an iteration index and $rand$ is a random number in (0, 1) that is uniformly distributed. Equations (8) and (9) are means of updating the new positions of streams which flow to rivers and the sea, respectively. Likewise, Equation (10) is the updated equation for the rivers that flow to the sea. If the solution given by a stream is better than that of its connecting river, there will be a swapping of positions between river and stream (i.e., stream replacing the position of river and river replacing the position of stream). Similarly, the swapping of positions can take place among rivers and seas. Fig.4 depicts the exchange of a stream, which is the best solution among other streams and the river.

c: EVAPORATION CONDITION

In this algorithm, evaporation is among the major features that can prevent early convergence. In the proposed method, the evaporation process causes the seawater to evaporate as rivers/streams flow to the sea. This assumption is proposed to avoid getting stuck in local optima. The following pseudo-code shows how to determine whether or not a river flows to the sea.

$$\begin{aligned} & \text{if } |X_{Sea}^i - X_{River}^i| < d_{max} \quad i = 1, 2, 3, \dots, N_{sr} - 1 \\ & \quad \text{Evaporation and raining process} \\ & \text{end} \end{aligned} \tag{11}$$

where d_{max} is a small number (close to zero). As a result, if the distance between a river and the sea is smaller than d_{max} , it implied that the river has reached/joined the sea. In this situation, the evaporation process is employed, and as witnessed in the real world, always adequate evaporation is the precondition for the rain (precipitation) to start. A large value for d_{max} minimizes the search, whereas a small value improves the search intensity close to the sea. Therefore, d_{max} is the parameter that controls the search intensity near the sea (the optimum solution). An adaptive minimization of

d_{max} value is achieved by employing (12) [70]:

$$d_{max}^{i+1} = d_{max}^i - \frac{d_{max}^i}{\text{Max. Iteration}} \quad (12)$$

where $i = 1, 2, \dots, \text{Max. Iteration}$

RAINING PROCESS

Once the evaporation process has sufficiently occurred, the next process to be utilized is the raining process. In this process, streams are formed at different sites due to the newly arriving raindrops. Equation (13) specifies the new locations of the newly formed streams;

$$X_{Stream}^{new} = LB + rand \times (UB - LB) \quad (13)$$

where LB and UB are the lower and upper bounds defined by the given problem, respectively. Again, the best newly formed raindrop is considered a river flowing to the sea. The remaining new raindrops are assumed to form new streams that flow to the rivers or may directly flow to the sea. To advance the convergence rate and computational performance of the algorithm for constrained problems, (14) is employed solely for the streams that move straight to the sea. Equation (14) main objective is to boost the formation of streams that flow right to the optimal position (sea) to advance the exploration close to the sea, which is the ideal solution in the feasible area for constrained problems.

$$X_{Stream}^{new} = X_{sea} + \sqrt{\mu} \times randn(1, N_{var}) \quad (14)$$

where μ is a coefficient that shows the range of the searching region near the sea. The variable $randn$ is the normally distributed random number. The larger value for μ increases the possibility of exiting the feasible region. On the contrary, the smaller value for μ leads the algorithm to search in a smaller region near the sea. A suitable value for μ is set to 0.1.

From a mathematical perspective, the square root of μ in (14) represents the standard deviation, and accordingly, μ defines the concept of variance. Based on these thoughts, the newly created entities with variance μ are distributed around the best-obtained optimum point (sea).

d: CONVERGENCE CRITERIA

In this proposed technique, the stopping conditions are the maximum number of iterations, a small non-negative value ϵ , which is set as a permitted tolerance between the very last two iteration results, or the period of time since the algorithm began running. Even if the convergence requirement is achieved before the maximum iteration, the WCA continues until the maximum number of iterations is reached.

To summarize, rivers (several best-chosen points excluding the sea, which is the best one) serve as “guidance points” in the WCA, minimizing or preventing searching in inappropriate areas in close proximity to optimal solutions (see (8)), as well as directing other members of the population towards better positions. Moreover, rivers are not stagnant in the system and are constantly flowing toward the best solution (the sea). This process (moving streams to rivers, then rivers

to the sea) results in an indirect motion in the direction of the ideal solution. In PSO, however, only individuals (particles) are able to determine the best approach to searching and the best solution based on their own unique experiences. Evaporation and raining conditions, which make up WCA’s two essential conditions, serve as a safeguards against the algorithm’s premature convergence. However, it appears that PSO lacks such standards or mechanisms.

Algorithm 1 WCA

```

Set parameters of WCA:  $N_{pop}$ ,  $N_{sr}$  and Maximum_
Iteration.
Determine the number of streams that flow to the rivers and
sea using (4) and (5)
Randomly create an initial population of streams.
Define the intensity of the flow using (6)
While ( $t < \text{Maximum\_Iteration}$ ) or (any stopping condi-
tion)
for  $i = 1$  : population size ( $N_{pop}$ )
stream flows to its corresponding rivers and sea using (8)
and (9) calculate the objective function of the generated
stream
    if  $F_{New\_Stream} < F_{river}$ 
        River=New_stream;
    if  $F_{New\_Stream} < F_{Sea}$ 
        Sea=New_Stream;
    end if
end if
River flows to the sea using (10)
Calculate the objective function of the generated river

    if  $F_{New\_River} < F_{Sea}$ 
        Sea = New_River;
    end if
end for
for  $i = 1$  : number of rivers ( $N_{sr}$ )
    if ( $norm(\text{Sea} - \text{River}) < d_{max}$ ) or ( $rand < 0.1$ ))
        New streams are created using (11)
    end if
end for
Reduce the  $d_{max}$  using (12)
end while

```

D. FUNCTIONS USED

To carry out an enhancement operation, a transformation function and a fitness function are utilized. The transformation function is employed to produce a new intensity value for the original image and generate an enhanced image. To evaluate the quality of the enhanced image, a fitness function is used.

1) TRANSFORMATION FUNCTION

Here I have applied the local enhancement method to a pixel, considering the intensity distribution among its neighboring pixels. Extraction of local information is done from

a user-defined window of size $n \times n$. The transformation function is given by (15)

$$g(i, j) = Z(i, j)[f(i, j) - c \times m(i, j)] + m(i, j)^a \quad (15)$$

In (15) a and c are two parameters, $m(i, j)$ is the local mean of the $(i, j)^{th}$ pixel of the input image over an $n \times n$ window and $Z(i, j)$ is enhancement function which takes both local and global information into account. An expression for local mean and enhancement function is defined as

$$m(i, j) = \frac{1}{n \times n} \sum_{x=1}^n \sum_{y=1}^n f(x, y) \quad (16)$$

$$Z(i, j) = k \left(\frac{G}{\sigma(i, j) + b} \right) \quad (17)$$

where k and b are two parameters, G is the global mean, and $\sigma(i, j)$ is the local standard deviation of $(i, j)^{th}$ pixel of the input image over an $n \times n$ window, which are defined as:

$$G = \frac{1}{N \times M} \sum_{x=1}^M \sum_{y=1}^N f(x, y) \quad (18)$$

where N and M are the numbers of pixels in the horizontal and vertical portions of an image, respectively.

$$\sigma(i, j) = \left(\frac{1}{n \times n} \sum_{x=1}^n \sum_{y=1}^n (f(x, y) - m(i, j))^2 \right)^{1/2} \quad (19)$$

Thus, the transformation function is

$$g(i, j) = \left(\frac{k \cdot G}{\sigma(i, j) + b} \right) [f(i, j) - c \times m(i, j)] + m(i, j)^a \quad (20)$$

Using (20), I stretched the contrast of the image, considering the local mean as the middle of the stretch. Parameters a , b , c , and k are introduced in the transformation function to get large variations in the processed image.

2) FITNESS CRITERION

One of the requirements of image enhancement is to choose a criterion that is related to a fitness function. This proposed method requires that the enhanced image must have a relatively high intensity of the edges. Consequently, the fitness criterion is proportional to the number and intensities of the pixels at the edges, might give an oversized credit to an image that does not have a natural contrast. In fact, we need a fitness criterion to evaluate the quality of the processed image with a uniform intensity distribution. The fitness function shown in (21), is used as an enhancement criterion:

$$F(I_{Enhanced}) = \log(\log(E(I_{Sobel}))) \frac{n_edge_I_{Sobel}}{M \times N} \times (H(I_{Enhanced})) \quad (21)$$

where $I_{Enhanced}$ is the enhanced image of the original image produced by the transformation function defined in (20), $(E(I_{Sobel}))$ is the sum of $M \times N$ pixel intensities of the Sobel

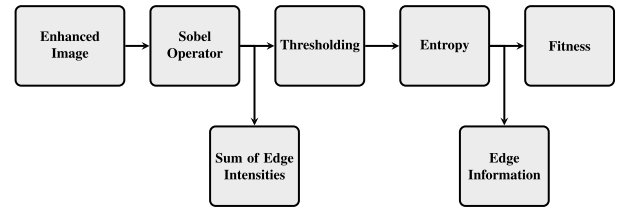


FIGURE 5. Extracting image information.

edge image I_{Sobel} , and $n_edge_I_{Sobel}$ is the number of edge pixels as detected with the Sobel edge detector. Thresholding offers a suitable way to execute segmentation of images based on differences in intensities or colors in the background and foreground of an image. In this study, the Sobel detector employs an automatic thresholding detector that performs the separation of edge pixels from non-edge pixels based on their intensity variation. Lastly, $H(I_{Enhanced})$ measures the entropy of the image.

E. EDGE DETECTION

Edges in an image are points where the gray value changes considerably from one pixel to another. They represent regions in the image with high-intensity contrasts (sharp changes in image brightness) [71], [72]. Representing an image by its edges has the fundamental advantage that the amount of data is reduced significantly while retaining most of the image's vital information with at high frequencies. Edges comprise important characteristics and contain significant information. Basically, images have a substantial amount of redundancies that can sometimes get rid of when edges are spotted and replaced, when they are reconstructed. When image edges are detected, every kind of redundancy present in the image is removed [73]. The process of locating an edge of an image is therefore called edge detection. Though there are several edge detection mechanisms, the Sobel operator's performance is better than others [72].

F. IMAGE ENHANCEMENT USING WCA

1) STEPS FOR IMPLEMENTATION

The steps of WCA are summarized as follows:

Step 1: Choose the initial parameters of the WCA: N_{sr} , d_{max} , N_{pop} , Maximum_Iteration.

Step 2: Calculate the Mean (16), Global Mean (18), and Standard Deviation (19).

Step 3: Generate a random initial population and form the initial streams (raindrops), rivers, and sea using (1), (4), and (5).

Step 4: Generate an enhanced image using (20).

Step 5: Calculate the fitness of each raindrop utilizing (21).

Step 6: Determine the intensity of flow for rivers and sea using (6).

Step 7: The streams flow to the rivers by (8).

Step 8: The streams flow to the sea by (9).

Step 9: The rivers flow to the sea which is the most downhill place employing (10).

Step 10: Exchange positions of the river with a stream that gives the best solution, as shown in Fig. 4.

Step 11: Similar to step 10, if a river finds a better solution than the sea, the position of the river is exchanged with the sea as illustrated in Fig. 4.

Step 12: Check the evaporation condition (11).

Step 13: If the evaporation condition is satisfied, the raining process will occur using (13) and (14).

Step 14: Reduce the value of d_{max} which is a user-defined parameter using (12).

Step 15: Check the convergence criteria. If the stopping criterion is satisfied, the algorithm will be stopped, otherwise return to Step 7.

Algorithm 2 Algorithm Used

Set parameters of WCA: N_{pop} , N_{sr} , Maximum_Iteration, and window size (n).

Read the image: Convert it into a gray image.

Calculate the Mean (16), Global Mean (18), and Standard Deviation (19).

for each particle $i = 1$: population size (N_{pop}) **do**
 initialize parameters a, b, c and k (randomly within their range) and corresponding random velocities.
end for

Generate enhanced image using (20)

Calculate fitness function value using (21).

Determine the number of streams which flow to the rivers and sea using (4) and (5).

Define the intensity of the flow using (6)

While ($t < \text{Maximum_Iteration}$) or (any stopping condition)

for $i = 1$: population size (N_{pop})
 stream flows to its corresponding rivers and sea using (8) and (9).
 calculate the objective function of the generated stream

if $F_{New_Stream} < F_{river}$

River=New_stream;

if $F_{New_Stream} < F_{Sea}$

Sea=New_Stream;

end if

end if

River flows to the sea using (10)

Calculate the objective function of the generated river

if $F_{New_River} < F_{Sea}$

Sea = New_River;

end if

end for

for $i = 1$: number of rivers (N_{sr})

if ($norm(Sea - River) < d_{max}$) or ($rand < 0.1$)

New streams are created using (11)

end if

end for

Reduce the d_{max} using (12)

end while

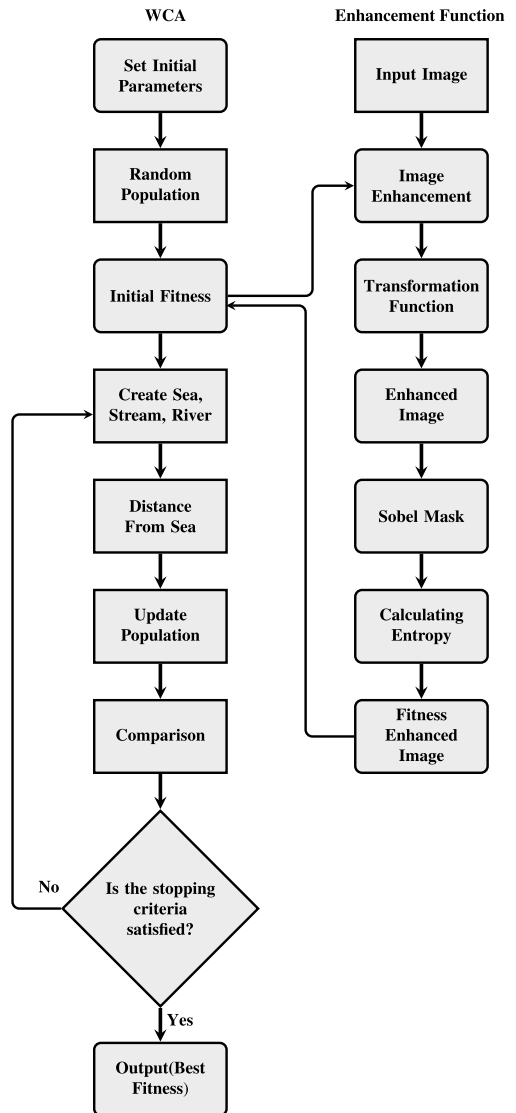


FIGURE 6. WCA Flow chart.

2) PARAMETER SETTINGS

For a better result of the WCA algorithm, $N_{sr} = 10$, $d_{max} = 1e - 5$ is used. In this study, there are four problem-specific parameters a, b, c and k . The ranges of these parameters are set as $a \in [0.8, 1.5]$, $b \in [1, 22]$, $c \in [0.01, 0.6]$, and $k \in [0.5, 2]$. The proposed technique’s experimental setup parameters, along with their values and range of values, are presented in Table 1.

The linear image transformation parameters a, b, c , and k are used to modify an image’s brightness and contrast. How each parameter affects the image is presented below:

- a : Adjusts the image’s contrast. The contrast is increased if $a > 1$ whereas the contrast is reduced if $a < 1$.
- b : Adjusts the image’s brightness. The brightness is raised if b is bigger than 0. When b is less than zero, the brightness is reduced.

TABLE 1. Experimental set up parameters.

S.No.	Parameter	Value
1	Maximum iteration	50
2	Number of population (N_{pop})	40
3	Variable size (N_{vr})	4
4	Window size	3×3
5	Number of river including sea (N_{sr})	10
6	d_{max}	$1e - 5$
7	a	[0.8, 1.5]
8	b	[1, 22]
9	c	[0.01, 0.6]
10	k	[0.5, 2]

- c : increase each image pixel's value by a constant value. This can be used to change the brightness of the image's dark parts.
- k : scales the image's pixel values. This allows you to modify the brightness of the bright portion of the image.
- Window size $n \times n$: In Sobel operator detection, the window size is the size of the kernel used to determine the gradient of the image. The kernel is a matrix that moves across the image, performing a convolution process. The more smoothing done to the image before computing the gradient, the larger the window size. This can result in reduced noise but also less detail in the output. Smaller window sizes, on the other hand, can produce greater detail but also more noise in the output.
- Population size N_{pop} : is one of the adjustable parameters in the suggested approach. The number of candidate solutions created in each iteration is determined by the population size. The larger the population size, the more candidate solutions are generated, increasing the possibility of finding a good solution but also increasing the computing cost.
- d_{max} : is another customizable parameter that controls the intensity of the search near the sea (the best solution). A big d_{max} value reduces the search, whereas a small value increases the search intensity near the sea.

G. IMAGE QUALITY ASSESSMENT (IQA) METRICS

Quantitative performance measurements are significant to determine how well the image is enhanced. The enhanced images are measured by defined IQA metrics to compare which enhancement technique is better. A detailed review of several image quality measurement metrics has been presented by Dhal et al. [56]. It is customary practice to use multiple image quality metrics as it signifies the quality of the image in terms of visual perception [15], [44], [49], [56], [74], [75], [76]. A brief description of the IQA metrics incorporated in this study is presented below. The IQA metrics along with their desirable values are depicted in Table 2.

1) NUMBER OF EDGE (N_g)

It is sometimes referred to as the sum of edge intensities. The number of edge pixels, N_g , in the enhanced image is

obtained as:

$$N_g = \sum_{i=1}^H \sum_{j=1}^V E_g(i, j) \quad (22)$$

2) ENTROPY

This is a popular evaluation function in image processing operations. Its value discloses the information contained in the image [77]. If the distribution of the intensities is uniform, then we can say that the histogram is equalized and the entropy of the image will be higher. $H(I_{Enhanced})$ is the entropy value that is calculated on the enhanced image $I_{Enhanced}$ as follows [77]:

$$E(I_{Enhanced}) = - \sum_{i=0}^{255} e_i \quad (23)$$

$$\text{where } e_i = \begin{cases} h_i \log_2(h_i) & \text{while } h_i \neq 0 \\ 0 & \text{otherwise} \end{cases}$$

h_i is the probability of occurrence i^{th} gray value.

3) CONTRAST

Contrast quantifies the intensity level difference among the pixels and their neighbors in the image. The higher the adjacent intensity level difference, the higher the contrast. The contrast of the image is calculated as

$$C = \sum_i \sum_j (i - j)^2 P(i, j) \quad (24)$$

where i and j are the two different gray levels of the image, P is the number of the co-appearance of the gray levels i and j .

4) MEAN SQUARED ERROR (MSE)

MSE is one of the most popular metrics in the image processing field due to its easy formulation and straightforward interpretation [78], [79], [80]. It is used to find out the occurrence of unwanted noise in the image. Assuming a noise-free $M \times N$ monochrome image where M and N are the height and width of the image, with f the original image and its enhanced version, which is a noisy approximation g , then MSE is defined as in (25).

$$\text{MSE} = \frac{1}{M \times N} \sum_{i=1}^M \sum_{j=1}^N |f(i, j) - g(i, j)|^2 \quad (25)$$

where $f(i, j)$ and $g(i, j)$ are the $(i, j)^{th}$ pixel value of the original image f and the distorted image g , respectively.

5) PEAK SIGNAL-TO-NOISE RATIO (PSNR)

PSNR of the image is determined by dividing the maximum signal power by the noise power, which corrupts the image and reduces its reliability. It is utilized to quantify the quality of reconstruction (enhancement in this case). In the image enhancement operation case, the signal is the original data, and the noise is the error produced in the enhancement

process. PSNR is considered an approximation to human perception of reconstruction quality. Even though a higher value of PSNR indicates that the enhancement process results in a better-quality image, sometimes this may not be true [15]. PSNR is defined via the MSE and is given by

$$PSNR = 10 \log_{10} \left[\frac{(L - 1)^2}{MSE} \right] \quad (26)$$

where MSE is given by (25) and L represent the maximum gray-scale image intensity level, which is 256.

6) ABSOLUTE MEAN-BRIGHTNESS ERROR (AMBE)

The image feature that is measured by AMBE is the degree of brightness preservation. Let the input image be f and the output image be g then the AMBE is given by (27):

$$AMBE = |mean(f) - mean(g)| \quad (27)$$

where, $mean(f)$ and $mean(g)$ are the mean of the reference and distorted (enhanced in this study) image, respectively. For better image brightness preservation, the desired AMBE value is low [81].

7) STRUCTURAL SIMILARITY (SSIM)

SSIM quantifies empirically the resemblance of two images: the original image and the enhanced or recovered image [79]. This metric came into existence since the widely used image quality assessment metrics such as PSNR and MSE do not consider the human visual system (HVS), and they show poor consistency with subjective evaluations [82]. The index evaluates the structural changes that have visual influences, such as shifts in luminance, the difference in contrast, and other remaining errors [78]. SSIM is mathematically expressed using the equation (28)

$$SSIM(f, g) = [l(f, g)]^\alpha \cdot [c(f, g)]^\beta \cdot [s(f, g)]^\gamma \quad (28)$$

where, f and g are the original image $f(i, j)$ and the enhanced image $g(i, j)$ respectively, l is the luminance (used to compare the brightness between the original image and its enhanced version), c is the contrast (employed to differ the intensity ranges between the brightest and darkest region of the original and enhanced image), and s is the structure (used to compare the local luminance pattern between two images to find the similarity and dissimilarities of the images), and α , β , and γ are the positive constants [78].

SSIM and its variants were developed based on the finding that the HVS is strongly adapted to extracting structural information from an image. Hence, these IQA metrics are a good measurement of structural similarity and are thereby considered a good estimate of perceived image quality.

8) MULTI-SCALE SSIM (MS-SSIM)

Wang et al. proposed the SSIM metric in 2004. According to Wang et al., investigation yielding blocking artifacts is the only drawback of SSIM [83]. To circumvent this problem, Wang et al. advanced SSIM and proposed MS-SSIM, which

yields a better performance than SSIM [84]. The MS-SSIM is defined as

$$MS-SSIM = \prod_{j=1}^M (SSIM_j)^{\beta_j} \quad (29)$$

where M is the number of scales and β_j the weight given to the j^{th} scale, which is obtained through psychophysical measurement.

9) INFORMATION CONTENT BASED IQA METRICS

These FR-IQA metrics were created with the concept that while seeing natural images, the best perceptual weights for pooling should be proportionate to the local information content. The local quality or distortion is measured in this scenario, and it is combined with the information content as the weighting parameter. The fundamental function of these metrics is to measure the local quality or distortion of a picture in the same way that MSE, PSNR, or SSIM do. Then, using the information content weighting, the new quality measures such as IW-MSE (information-weighted MSE), IW-PSNR, or IW-SSIM are computed [85].

Let $f(i, j)_j$ and $g(i, j)_j$ be the transform coefficients at the j^{th} scale, and $w_{j,i}$ be the information content weight computed at the corresponding location, then we define IW-MSE as [86]

$$IW-MSE = \prod_{j=1}^M \left[\frac{\sum_i w_{j,i} (f(i, j)_j - g(i, j)_j)^2}{\sum_i w_{j,i}} \right]^{\beta_j} \quad (30)$$

where M is the number of scales, β_j is the weight given to the scale, and the weights are defined in similar ways as in the MS-SSIM case.

In a similar way to the MSE-PSNR conversion, IW-PSNR can be derived from IW-MSE as [86]

$$IW-PSNR = 10 \log_{10} \left[\frac{(L - 1)^2}{IW-MSE} \right] \quad (31)$$

We construct an information content weighted SSIM measure (IW-SSIM) by merging information content weighting and multiscale SSIM [86]. Let $w_{j,i}$ be the information content weight computed at the spatial location in the j^{th} scale, then the j^{th} scale IW-SSIM measure is defined as

$$IW-SSIM_j = \frac{1}{N_j} \sum_{j=1}^M [l(f, g)]^\alpha \cdot [c(f, g)]^\beta \cdot [s(f, g)]^\gamma \quad (32)$$

for $j = M$. The final overall IW-SSIM measure is then computed as

$$IW-SSIM = \prod_{j=1}^M (IW - SSIM_j)^{\beta_j} \quad (33)$$

using the same set of scale weights β_j 's as in MS-SSIM.

10) FEATURE SIMILARITY (FSIM)

The Feature Similarity (FSIM) index for FR-IQA was proposed by Zhang et al. [84] depending on how a human visual system (HVS) recognizes an image due to its low-level features. The two main low-level features in FSIM are phase congruency (PC), which is the primary feature, and gradient magnitude (GM), which is the second feature [83]. PC is a unitless measure of the importance of the local structure of an image. PC and GM oppositely characterize the image's local quality. A single quality score is obtained by employing PC as a weighting function on a predetermined local quality map. In terms of subjective evaluation, FSIM shows much higher reliability than other metrics. In addition to this, FSIM is devised for grayscale image quality assessment purposes [83], [84]. A detailed discussion of FSIM is found in [83].

11) INFORMATION FIDELITY CRITERIA (IFC)

This is a natural scene statistics (NSS) model-based IQA metric that utilizes the amount of visual information that exists in the image. There is a strong statistical relationship between pixels in natural images. This relationship is believed to be disturbed by distortions and to deviate from its original form [87]. In these metrics, the combination of NSS and distortion models is the basis for fidelity measurement. In the wavelet domain, the reference image is modeled as an NSS, and the distortion model is taken as an attenuation and additive Gaussian noise model. The fidelity criterion between the source and distorted images is the mutual information shared by them.

12) VISUAL INFORMATION FIDELITY (VIF)

Sheikh and Bovik developed an IQA metric that is an extension of IFC and measures the information present in the original reference image and to what extent this information is extracted from the distorted image [88]. These two information measurements were combined and a new IQA metric for visual information fidelity was developed. The VIF value lies in the interval [0,1] where 0 indicates that all the information present in the reference image is lost and not found in the distorted image whereas a VIF value of 1 indicates that all the information present in the reference image is found in the image that is assumed distorted.

To test the effectiveness of the proposed image enhancement techniques, several FR-IQA metrics were used. These FR-IQA measurements are divided into two categories. The first category includes signal fidelity measurement metrics such as MSE, PSNR, and AMBE. The second category includes perceptual visual quality measurements such as SSIM, MS-SSIM, IW-SSIM, IW-MSE, IW-PSNR, IFC, VIF, and FSIM. Despite the fact that physical differences in the first group measures reflect a change in image quality, these traditional and basic signal fidelity metrics fail to predict HVS perception. The latter group of measurements, on the other

TABLE 2. Image quality assessment (IQA) metrics.

S.No.	IQA metrics	Desired values
1	Number of detected edges	Higher
2	Entropy	Higher
3	Contrast	Higher
4	MSE	Lower
5	PSNR	Higher
6	AMBE	Lower
7	SSIM	Higher
8	MS-SSIM	Higher
9	IW-SSIM	Higher
10	IW-MSE	Lower
11	IW-PSNR	Higher
12	IFC	Higher
13	VIF	Higher
14	FSIM	Higher
15	Fitness	Higher

hand, is more dependable in gauging image quality because it is very good at predicting HVS.

Since the human visual system (HVS) is the ultimate user of processed pictures, video, and graphics, using a perceptual quality measure in image quality assessment would be more convincing and reasonable. This is the primary criterion for picking the previously mentioned FR-IQA measures.

III. RESULT AND DISCUSSION

This section presented the results (Tables 3, 4, 5, and 6 and Fig. 7-17), obtained from the computational work of this study. The MATLAB 2023a software was used to design the enhancement method and carry out all the analyses. All experiments were carried out on a computer system running Windows 10 with the 64-bit operating system. The system has 16 GB of random-access memory (RAM) and an Intel Core i7-4790 CPU at 3.60 GHz.

The main objective of this investigation was to enhance the given image using the WCA and extract image information with proper image enhancement. In this study, the objective function was formed by combining three performance measures, namely, entropy value, number of edges, and fitness of the image. To further test the performance of the proposed image enhancement method, 11 FR-IQA metrics were also used.

Sub-figure (a) and (b) of Fig. 7-17 showed 11 different reference and test images, respectively, that were used in this study. These images had sizes ranging from 190×304 to 380×445 .

A. SUBJECTIVE EVALUATION

In this subsection 11 different test images were enhanced and obtained results were depicted in Fig. 7-17. In these figures, reference image, test image, and images enhanced by HE, LCS, CLAHE, LCM-CLAHE, PSO, APSO, and proposed WCA were displayed side by side from left to right.

Sub-figures (c)-(i) showed that all the applied techniques improved the visual impression of the test image to

TABLE 3. IQA metrics comparison of the proposed technique with PSO, APSO, HE, and its variants.

Image (Figure No.)	Image Size ($M \times N$)	IQA Metrics	Image Enhancement Techniques						
			HE	LCS	CLAHE	LCM-CLAHE	PSO	APSO	Proposed
Bag (7)	300 × 428	Sum of Edge Intensities	4985	4369	4986	6025	381780	389260	445930
		Entropy	4.61	3.70	6.54	4.83	6.98	6.660	7.124
		Contrast	15.53	7.06	15.97	11.81	15.39	15.45	15.46
		Fitness	0.12	0.0701	0.144	0.118	0.458	0.4558	0.4615
Fruits (8)	220 × 293	Sum of Edge Intensities	2025	2317	2347	2723	229780	229820	232960
		Entropy	5.633	4.869	7.161	5.96	7.554	7.555	7.589
		Contrast	15.54	12.73	15.97	13.55	15.906	15.906	15.912
		Fitness	0.0919	0.0922	0.138	0.145	0.3866	0.3864	0.3866
Indoor (9)	320 × 488	Sum of Edge Intensities	8070	7058	7984	7784	497563	497376	497481
		Entropy	5.435	4.565	7.002	5.592	7.351	7.351	7.351
		Contrast	15.576	11.014	15.963	13.006	15.934	15.934	15.934
		Fitness	0.166	0.121	0.212	0.1824	0.4511	0.4484	0.4512
Car (10)	190 × 304	Sum of Edge Intensities	2966	2919	3118	3090	251110	251096	256490
		Entropy	4.581	3.72	6.372	4.71	6.267	6.267	7.292
		Contrast	15.545	9.65	15.97	12.82	15.595	15.5948	15.757
		Fitness	0.1272	0.1015	0.1869	0.1456	0.451115	0.451113	0.451115
Clock (11)	330 × 440	Sum of Edge Intensities	7384	7460	7133	8196	772203	773179	849868
		Entropy	5.238	4.484	7.035	5.1595	7.53	7.53	7.626
		Contrast	15.60	9.679	15.968	12.186	15.838	15.838	15.77
		Fitness	0.1565	0.1355	0.2024	0.1684	0.4466	0.4465	0.4467
Hall (12)	190 × 304	Sum of Edge Intensities	2883	3127	2848	3412	239600	234943	245180
		Entropy	5.144	4.235	6.823	4.803	7.605	7.610	7.757
		Contrast	15.574	9.459	15.967	11.817	15.768	15.774	15.737
		Fitness	0.1384	0.1246	0.1811	0.1535	0.44976	0.4494	0.45354
Face (13)	380 × 445	Sum of Edge Intensities	5604	4271	4110	5246	540730	544850	545280
		Entropy	5.0428	4.145	6.373	5.007	7.19	7.195	7.395
		Contrast	15.545	13.40	15.965	13.869	15.90	15.903	15.964
		Fitness	0.0959	0.0586	0.0864	0.0886	0.4678	0.46798	0.46798
Pencil (14)	190 × 304	Sum of Edge Intensities	1941	1610	1635	2074	298580	298320	298840
		Entropy	4.412	3.61	6.210	5.1849	6.767	6.91	6.729
		Contrast	15.536	14.82	15.969	14.986	15.951	15.957	15.96
		Fitness	0.077	0.051	0.089	0.095	0.4546	0.4547	0.4547
Flower (15)	300 × 310	Sum of Edge Intensities	2855	2810	3000	3577	496656	508469	552889
		Entropy	4.4238	3.596	6.432	4.8564	6.980	6.980	6.982
		Contrast	15.969	5.7397	15.967	10.39	14.83	14.846	14.854
		Fitness	0.073	0.058	0.112	0.103	0.4627	0.46351	0.4637
Circuit (16)	250 × 400	Sum of Edge Intensities	8160	10811	9586	11188	3034631	3142713	3051672
		Entropy	4.167	3.3975	6.4139	5.496	6.993	6.98	6.994
		Contrast	15.559	6.273	15.965	9.602	15.14	15.112	15.139
		Fitness	0.152	0.168	0.278	0.219	0.49689	0.49677	0.49677
Medical Image (17)	330 × 440	Sum of Edge Intensities	6153	5888	7064	6195	4027986	3805603	4812772
		Entropy	3.575	4.439	4.906	4.571	4.22	4.22	7.262
		Contrast	15.969	10.398	15.969	10.623	11.364	11.364	14.211
		Fitness	0.0615	0.0728	0.098	0.0793	0.5039	0.5048	0.5078

varying degrees. The hidden details in the test image were revealed with the HE, CLAHE, LCM-CLAHE, PSO, APSO, and WCA. However, the overall level of brightness was fair in CLAHE, PSO, APSO, and WCA-enhanced images. Whereas, HE resulted in an image with a high brightness level. On the contrary, LCM-CLAHE and LCS resulted in dark-enhanced images. The latter, LCS, even results in a more

darker enhanced image that did not give a chance for an obscure detail to be distinguished significantly. This enhancement phenomenon was found consistent almost with all test images.

The CLAHE, PSO, APSO, and WCA demonstrated better performance in detail enhancement and visual effect improvement than the aforementioned techniques.

TABLE 4. FR- IQA metrics comparison of the proposed technique with PSO, APSO, HE, and its variants.

Image (Figure No.)	Image Size (M × N)	IQA Metrics	Image Enhancement Techniques						
			HE	LCS	CLAHE	LCM-CLAHE	PSO	APSO	Proposed
Bag (7)	300 × 428	MSE	6030	4056	339	2719	324	354	290
		PSNR	10.33	12.05	22.82	13.79	23.01	22.628	23.50
		AMBE	68.26	52.83	4.06	44.82	13.16	14.20	12.01
		SSIM	0.5960	0.216	0.7763	0.3300	0.781	0.772	0.7881
		MS-SSIM	0.5960	0.2157	0.7763	0.3300	0.950	0.9478	0.9527
		IW-SSIM	0.7767	0.246	0.902	0.619	0.9481	0.9466	0.9498
		IW-MSE	3010	3369	374	1858	345	344	330
		IW-PSNR	13.34	12.86	22.39	15.44	22.74	22.755	22.945
		VIF	0.711	0.1193	0.5714	0.3565	0.4586	0.42	0.47
		IFC	4.5122	4.0625	4.8858	3.6263	2.9260	2.6980	3.1714
FSIM	0.8627	0.6172	0.9179	0.7760	0.9066	0.9046	0.9086		
Fruits (8)	220 × 293	MSE	987	12651	1388	9227	577	576	498
		PSNR	18.19	7.11	16.71	8.48	20.52	20.5227	21.15
		AMBE	7.6	105	27.6	91.94	17.71	17.69	14.44
		SSIM	0.8257	0.1066	0.8449	0.2958	0.7380	0.7380	0.7452
		MS-SSIM	0.8972	0.3852	0.9067	0.7271	0.9228	0.9226	0.9230
		IW-SSIM	0.9054	0.29	0.87	0.67	0.925	0.925	0.926
		IW-MSE	1192	4943	622	2555	490	489	486
		IW-PSNR	17.37	11.19	20.19	14.06	21.23	21.23	21.26
		VIF	0.58	0.177	0.57	0.39	0.3719	0.372	0.3712
		IFC	5.01	5.04	5.32	4.01	3.28	3.27	3.25
FSIM	0.9058	0.5069	0.9153	0.7464	0.8527	0.8529	0.8544		
Indoor (9)	320 × 488	MSE	1100	11867	1355	8520	334	334	332
		PSNR	17.72	7.387	16.80	8.83	22.885	22.886	23.03
		AMBE	15	100	27	88	3.482	3.485	3.478
		SSIM	0.868	0.102	0.8415	0.270	0.7847	0.7847	0.7847
		MS-SSIM	0.918	0.404	0.914	0.713	0.9293	0.9293	0.9293
		IW-SSIM	0.924	0.253	0.915	0.600	0.9286	0.9286	0.9286
		IW-MSE	894	4613	554	2538	400	400	400
		IW-PSNR	18.618	11.49	20.69	14.09	22.1	22.1	22.1
		VIF	0.629	0.173	0.559	0.345	0.371	0.371	0.371
		IFC	5.108	4.705	5.168	3.479	2.9465	2.9464	2.9465
FSIM	0.9281	0.5215	0.903	0.7208	0.8560	0.8560	0.8560		
Car (10)	190 × 304	MSE	2108	9294	2017	7189	1324	1324	1922
		PSNR	14.89	8.45	15.08	9.564	16.9	16.9	15.29
		AMBE	30.87	87.86	30.39	78.76	31.897	31.897	32.68
		SSIM	0.787	0.105	0.779	0.239	0.702	0.702	0.852
		MS-SSIM	0.8358	0.4162	0.7975	0.6545	0.879	0.879	0.919
		IW-SSIM	0.8386	0.213	0.828	0.511	0.8413	0.8413	0.9277
		IW-MSE	1767	4463	700	2993	1049	1049	686
		IW-PSNR	15.657	11.634	19.675	13.369	17.919	17.920	19.765
		VIF	0.5185	0.1471	0.5438	0.3173	0.3294	0.3294	0.5529
		IFC	3.635	4.484	4.634	3.104	2.4923	2.4922	3.95
FSIM	0.8739	0.5168	0.8819	0.6657	0.8234	0.8234	0.9214		
Clock (11)	330 × 440	MSE	1540	10068	587	7227	543	543	163
		PSNR	16.26	8.10	20.44	9.54	20.785	20.78	25.99
		AMBE	32.65	86.04	7.89	75.04	0.53	0.52	1.56
		SSIM	0.9172	0.0525	0.8686	0.2102	0.7333	0.733	0.9297
		MS-SSIM	0.951	0.2647	0.924	0.581	0.9392	0.9329	0.977
		IW-SSIM	0.9432	0.2050	0.9126	0.5552	0.9352	0.9352	0.9773
		IW-MSE	1117	8686	1006	5247	570	570	205
		IW-PSNR	17.648	8.7422	18.102	10.932	20.569	20.568	25.012
		VIF	0.604	0.2108	0.583	0.376	0.350	0.350	0.5486
		IFC	7.721	7.681	8.243	5.672	4.392	4.392	7.105
FSIM	0.9411	0.3509	0.9041	0.6020	0.8266	0.8265	0.9483		
Hall (12)	190 × 304	MSE	2084	8916	1015	6502	1682	1504	1354
		PSNR	14.94	8.629	18.06	10.00	15.87	16.36	16.813
		AMBE	38.823	80.93	11.44	70.998	29.56	30.11	27.66
		SSIM	0.8707	0.06498	0.8162	0.2065	0.7556	0.815	0.8547
		MS-SSIM	0.9437	0.28875	0.872	0.582	0.918	0.938	0.9443
		IW-SSIM	0.94175	0.1825	0.9022	0.5054	0.9263	0.9434	0.9468
		IW-MSE	940	7003	579	4454	821	636	620
		IW-PSNR	18.399	9.677	20.504	11.643	18.985	20.093	20.807
		VIF	0.6259	0.1747	0.5466	0.318	0.3798	0.424	0.472
		IFC	6.1345	5.6789	5.8961	3.6999	3.6204	4.0461	4.5231
FSIM	0.9441	0.3774	0.8909	0.6034	0.8660	0.8996	0.9209		

TABLE 5. FR-IQA metrics comparison of the proposed technique with PSO, APSO, HE, and its variants.

Image (Figure No.)	Image Size ($M \times N$)	IQA Metrics	Image Enhancement Techniques						
			HE	LCS	CLAHE	LCM-CLAHE	PSO	APSO	Proposed
Face (13)	380 × 445	MSE	1634	15686	4333	11980	3355	3439	2538
		PSNR	15.99	6.176	11.76	7.35	12.87	12.766	14.09
		AMBE	6.7375	119.157	54.783	105.469	55.353	57.058	45.444
		SSIM	0.638	0.1686	0.7734	0.3168	0.8262	0.8095	0.8592
		MS-SSIM	0.848	0.6118	0.8533	0.74296	0.9092	0.9098	0.9512
		IW-SSIM	0.8300	0.332	0.8659	0.5722	0.9246	0.9256	0.9497
		IW-MSE	783	3481	587	2595	340	344	166
		IW-PSNR	19.19	12.71	20.44	13.988	22.818	22.762	25.92
		VIF	0.5613	0.1178	0.5285	0.2334	0.4938	0.486	0.5246
		IFC	2.883	2.815	3.252	1.951	2.31	2.3005	2.488
FSIM	0.8301	0.6660	0.9111	0.7341	0.9084	0.9097	0.9167		
Pencil (14)	190 × 304	MSE	5341	4070	477	2125	10776	12415	129
		PSNR	10.8543	12.034	21.34	14.857	7.806	7.1912	27.025
		AMBE	54.23	57.95	0.39	42.62	101.77	109.05	7.17
		SSIM	0.5402	0.3261	0.8118	0.6525	0.5814	0.5499	0.8221
		MS-SSIM	0.6569	0.5708	0.8523	0.8390	0.8812	0.8490	0.9338
		IW-SSIM	0.6549	0.3546	0.8778	0.7584	0.8346	0.817	0.9383
		IW-MSE	5687	2807	585	1265	2410	2556	238
		IW-PSNR	10.58	13.65	20.46	17.11	14.31	14.05	24.35
		VIF	0.5806	0.1675	0.5263	0.4336	0.5604	0.5264	0.5636
		IFC	2.465	3.115	3.042	3.051	2.586	2.337	2.669
FSIM	0.7799	0.7403	0.9024	0.8818	0.8559	0.8735	0.8796		
Flower (15)	300 × 310	MSE	5955	4305	223	2930	238	248	232
		PSNR	10.38	11.79	24.63	13.46	24.37	24.17	24.46
		AMBE	68.238	55.1	3.45	47.3	0.95	2.43	0.39
		SSIM	0.584	0.1568	0.8211	0.2882	0.8894	0.8939	0.890
		MS-SSIM	0.8190	0.3415	0.9361	0.6430	0.9501	0.9499	0.9505
		IW-SSIM	0.8032	0.2186	0.9349	0.6196	0.9349	0.9349	0.9355
		IW-MSE	3104	3878	415	2024	644	655	631
		IW-PSNR	13.21	12.24	21.94	15.07	20.04	19.97	20.13
		VIF	0.6436	0.1245	0.6023	0.3661	0.5084	0.513	0.508
		IFC	3.899	3.81	4.85	3.41	3.30	3.34	3.32
FSIM	0.8619	0.6466	0.9354	0.8031	0.925	0.9256	0.926		
Circuit (16)	300 × 442	MSE	7667	4047	817	2631	766	764	766
		PSNR	9.284	12.059	19.00	13.929	19.286	19.298	19.286
		AMBE	79.54	43.696	12.319	36.815	12.5929	12.125	12.5928
		SSIM	0.4656	0.1575	0.6325	0.2348	0.76485	0.7638	0.7659
		MS-SSIM	0.8367	0.2999	0.8294	0.605	0.93338	0.9325	0.9334
		IW-SSIM	0.8009	0.1746	0.8066	0.5319	0.92615	0.9252	0.9263
		IW-MSE	3511	5898	1462	3437	1221	1241	1221
		IW-PSNR	12.68	10.42	16.48	12.77	17.26	17.19	17.29
		VIF	0.373	0.173	0.479	0.436	0.406	0.405	0.406
		IFC	3.673	6.723	5.585	6.552	4.149	4.13	4.149
FSIM	0.8173	0.3672	0.8116	0.6308	0.8394	0.8384	0.8395		
Medical Image (17)	330 × 440	MSE	3638	16418	7395	10848	4844	4844	4607
		PSNR	12.52	5.98	9.44	7.78	11.28	11.28	11.5
		AMBE	20	110	69	90	43	43	58
		SSIM	0.4199	0.1684	0.3204	0.2283	0.3011	0.3011	0.4699
		MS-SSIM	0.61	0.51	0.59	0.62	0.64	0.64	0.79
		IW-SSIM	0.60	0.47	0.61	0.60	0.65	0.65	0.80
		IW-MSE	6410	12784	8470	8800	8095	8095	3801
		IW-PSNR	10.06	7.06	8.85	8.69	9.048	9.05	12.33
		VIF	0.154	0.135	0.152	0.150	0.0898	0.0898	0.296
		IFC	1.89	1.76	1.71	1.69	0.98	0.98	3.64
FSIM	0.6598	0.5987	0.6324	0.5922	0.6428	0.6428	0.8022		

B. OBJECTIVE EVALUATION

The test images, depicted in sub-figure (b) of Fig. 7-17 were tested for objective quality evaluation using various IQA metrics. Three different IQA metrics, namely, contrast, entropy, the sum of edge intensities, and Fitness objective evaluation employed in this objective evaluation experiment. The obtained result was presented in Table 3 which indicated the best scores in terms of each mentioned metric.

The experimental results obtained on ‘Bag’, ‘Fruits’, ‘Indoor’, ‘Car’, ‘Clock’, and ‘Hall’ are shown in Table 4. Similarly, Table 5 showed the experimental result obtained through processing the test images ‘Face’, ‘Pencil’, ‘Flower’, ‘Circuit’, and ‘Medical image’. The best scores in terms of each metric are highlighted in both tables. These tabulated data presented that the different evaluation metrics assign different scores to the same image enhancement algorithm

TABLE 6. Running time comparison.

Number of Iterations		Image Enhancement Techniques						
		HE	LCS	CLAHE	LCM-CLAHE	PSO	APSO	Proposed
1	Average running time (second)	0.527	0.2715	0.2718	0.6127	9.29	8.34	9.7
50		64.41	62.14	153.24				

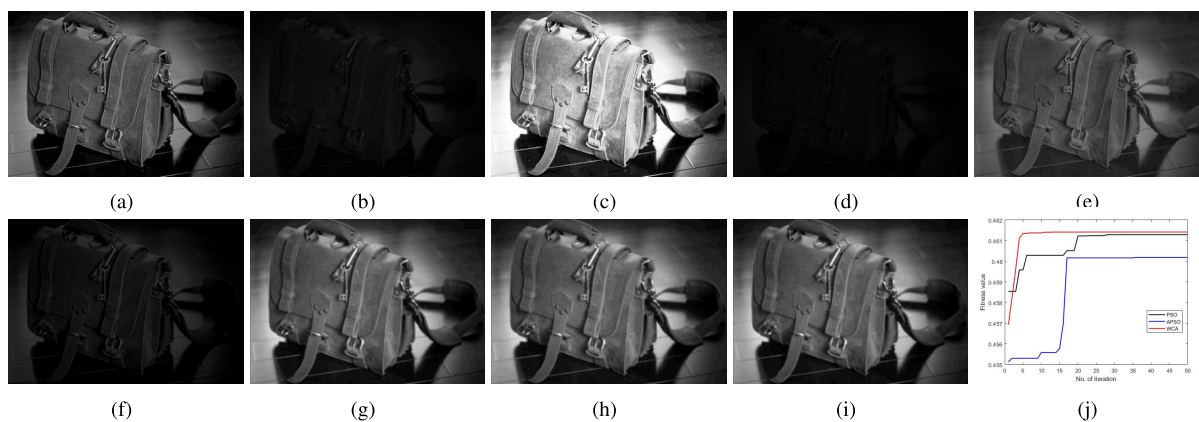


FIGURE 7. Bag images (a) Reference image (b) Test Image (c) HE (d) LCS (e) CLAHE (f) LCM-CLAHE (g) PSO (h) APSO (i) WCA (j) Fitness plot.

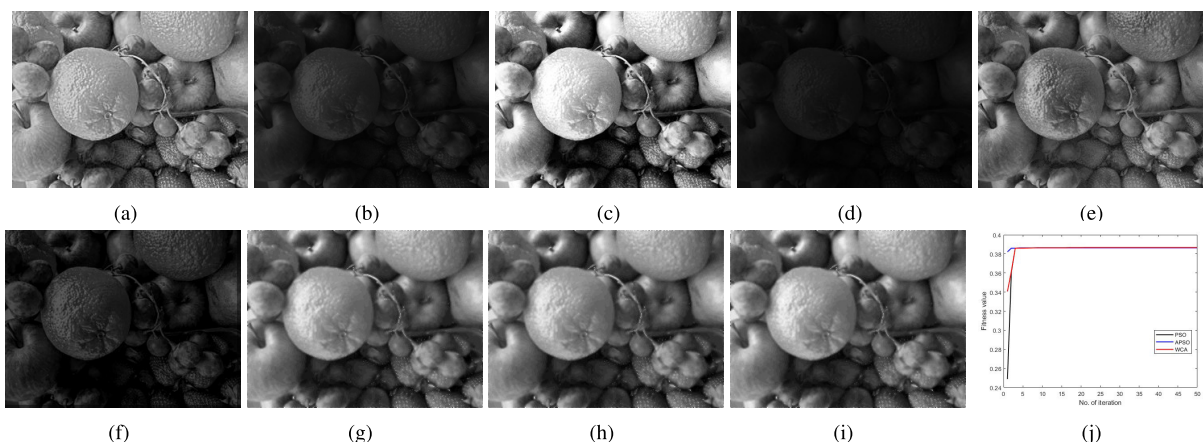


FIGURE 8. Fruits images (a) Reference image (b) Test Image (c) HE (d) LCS (e) CLAHE (f) LCM-CLAHE (g) PSO (h) APSO (i) WCA (j) Fitness plot.

and that the interpretations of the evaluation results were entirely opposite in some cases.

The comparison based on the metrics with fitness and its constituents, sum of edge intensities, contrast and entropy, is presented in Table 3. Accordingly, the proposed method (WCA) attained the best score for all images with respect to sum of the edge intensities metric and objective function fitness. This method also performed better than all the remaining techniques in terms of entropy for all, except ‘Flower’ and ‘Pencil’, test images. However, in terms of the metric contrast, the suggested method scored the second best value for ‘Fruits’, ‘Indoor’, ‘Car’, ‘Face’, and ‘Pencil’, the third for ‘Bag’, ‘Flower’, and ‘Medical image’ test images.

The obtained results (Tables 4 and 5) generally indicated that none of the applied techniques provided the highest score for all test images in terms of all 11 FR IQA metrics.

According to metrics MSE and its derivative (PSNR), the proposed technique scored the best value in enhancing images of ‘Bag’, ‘Fruits’, ‘Indoor’, ‘Clock’, and ‘Pencil’. Whereas it scored the second best value for all, except ‘Circuit’, remaining images. This also implied that the error and distortion created in the process of enhancing the test images were minimum and do not reflected in the enhanced images. On the contrary, in the majority of the test images LCS showed high MSE value and the least PSNR value.

The LCM-CLAHE technique achieved the highest score in terms of PSNR for almost all images except for the test image ‘Car’. Besides the proposed method achieved the second highest score (next to LCM-CLAHE) for all the remaining test images using the same metric.

The proposed method was found with the best AMBE value for ‘Indoor’, and ‘Flower’; second best for ‘Bag’,



FIGURE 9. Indoor images (a) Reference image (b) Test Image (c) HE (d) LCS (e) CLAHE (f) LCM-CLAHE (g) PSO (h) APSO (i) WCA (j) Fitness plot.

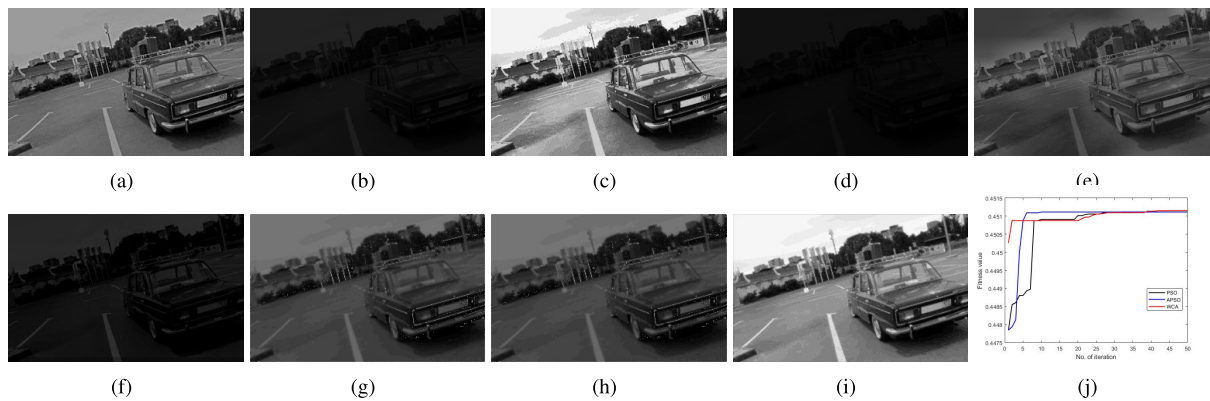


FIGURE 10. Car images (a) Reference image (b) Test Image (c) HE (d) LCS (e) CLAHE (f) LCM-CLAHE (g) PSO (h) APSO (i) WCA (j) Fitness plot.

‘Fruit’, ‘Hall’, ‘Face’, and ‘Pencil’; third best for ‘Clock’, ‘Circuit’, and ‘Medical images’. Hence, it can generally be considered as the second-best technique. This asserts that the proposed technique achieved one of its goals, which was to preserve the brightness of the images.

This WCA-based method also showed the best performance in enhancing the test images ‘Bag’, ‘Car’, ‘Clock’, ‘Face’, ‘Pencils’, ‘Circuit’, and ‘Medical image’ with respect to the SSIM evaluation metric (Tables 4 and 5). With this metric the method scored the second and third best value in enhancing the test images ‘Hall’, and ‘Flower’, and ‘Fruits’, and ‘Indoor’, respectively.

The suggested method demonstrated a remarkable and consistent performance across all test images in terms of MS-SSIM and IW-SSIM metrics. The method also achieved the best IW-MSE and IW-PSNR values in enhancing all test images except for ‘Flower’, which scored the second best value.

The proposed method (WCA), with respect to the VIFIQA metrics, also exhibited the best performance in enhancing ‘Car’ and ‘Medical image’; whereas it scored the third best value for ‘Bag’, ‘Fruits’, ‘Indoor’, ‘Clock’, ‘Hall’, ‘Face’, ‘Pencil’, and ‘Flower’ test images.

With reference to the IFC metric, the studied method (WCA) was ranked first in its enhancing performance for ‘Medical image’, third for ‘Car’, and fourth for ‘Hall’, ‘Clock’, ‘Face’, ‘Pencil’, and ‘Circuit’ test images. Whereas it was found with below-average performance for the remaining test images compared to the other six techniques.

According to the obtained FSIM performance measurement result, the proposed method (WCA) was found to produce a comparatively good-quality of image enhancement. That is, it provided the highest FSIM score in enhancing ‘Car’, ‘Clock’, ‘Face’, ‘Circuit’, and ‘Medical image’ test images. Whereas the method was found second for ‘Bag’, ‘Hall’, ‘Pencil’, and ‘Flower’; and third for ‘Fruits’, and ‘Indoor’ test images.

C. IMAGE ENHANCEMENT COMPARISON BETWEEN WCA, PSO AND APSO

All the test images were enhanced with a maximum number iterations of 50 and a population size of 40 for the three NIA-based image enhancement methods. As it was presented in the previous subsection B, the proposed method showed a performance better than PSO and APSO for all test images

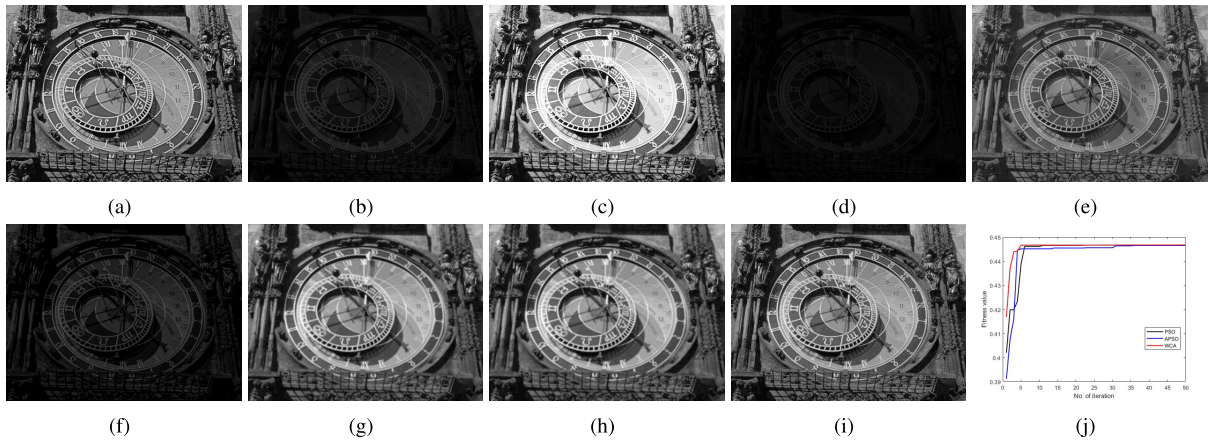


FIGURE 11. Clock images (a) Reference image (b) Test Image (c) HE (d) LCS (e) CLAHE (f) LCM-CLAHE (g) PSO (h) APSO (i) WCA (j) Fitness plot.

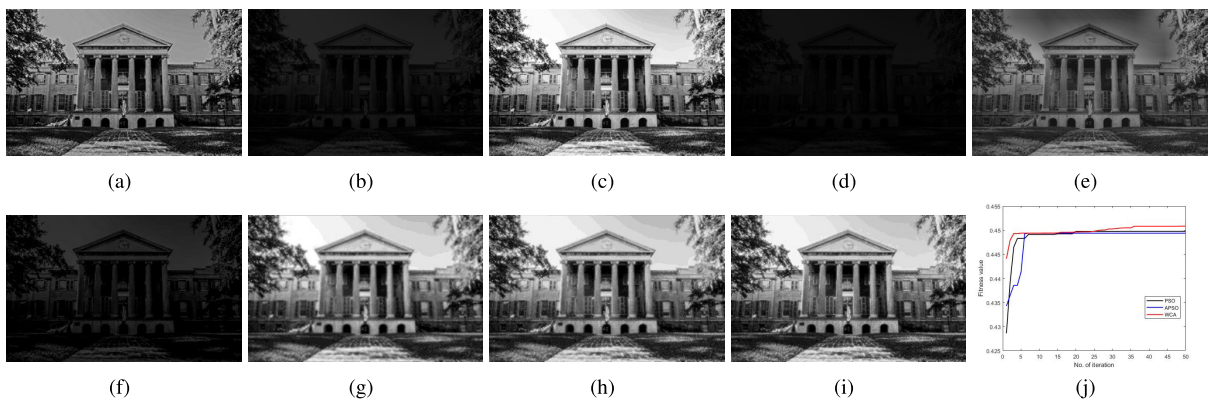


FIGURE 12. Hall images (a) Reference image (b) Test Image (c) HE (d) LCS (e) CLAHE (f) LCM-CLAHE (g) PSO (h) APSO (i) WCA (j) Fitness plot.

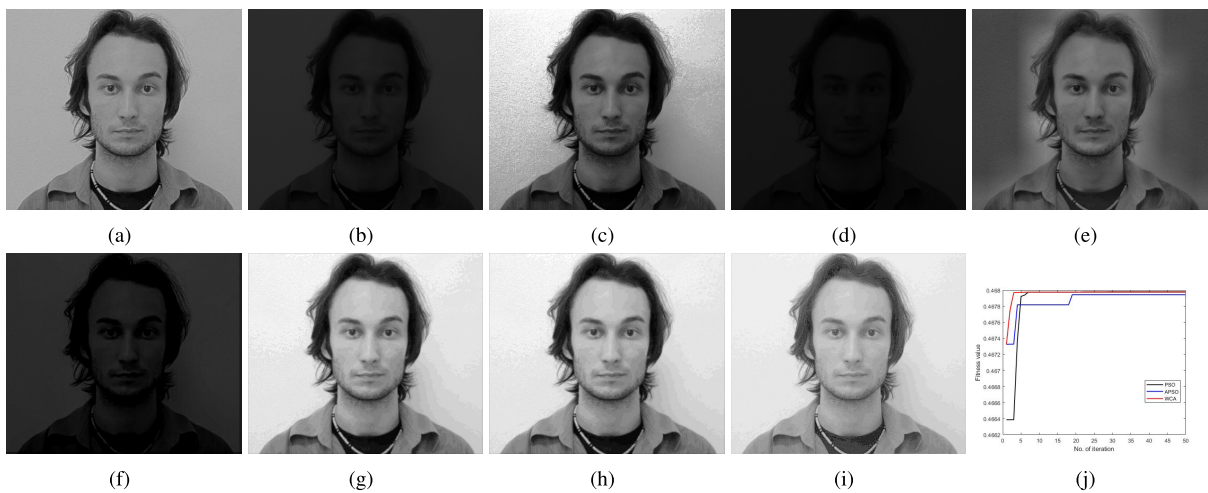


FIGURE 13. Face images (a) Reference image (b) Test Image (c) HE (d) LCS (e) CLAHE (f) LCM-CLAHE (g) PSO (h) APSO (i) WCA (j) Fitness plot.

in terms of the metric sum of edge intensities and objective function fitness. The method also performed better than the above two techniques in enhancing all but ‘Indoor’, and

‘Pencil’ test images with respect to the entropy measurement. On top of this, the proposed method was found with better performance in terms of MSE and PSNR than PSO and APSO

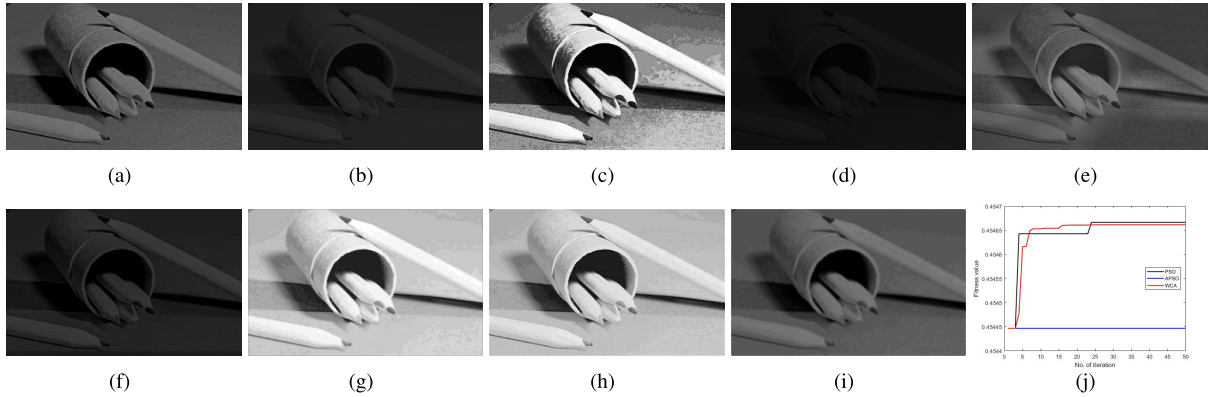


FIGURE 14. Pencil images (a) Reference image (b) Test Image (c) HE (d) LCS (e) CLAHE (f) LCM-CLAHE (g) PSO (h) APSO (i) WCA (j) Fitness plot.

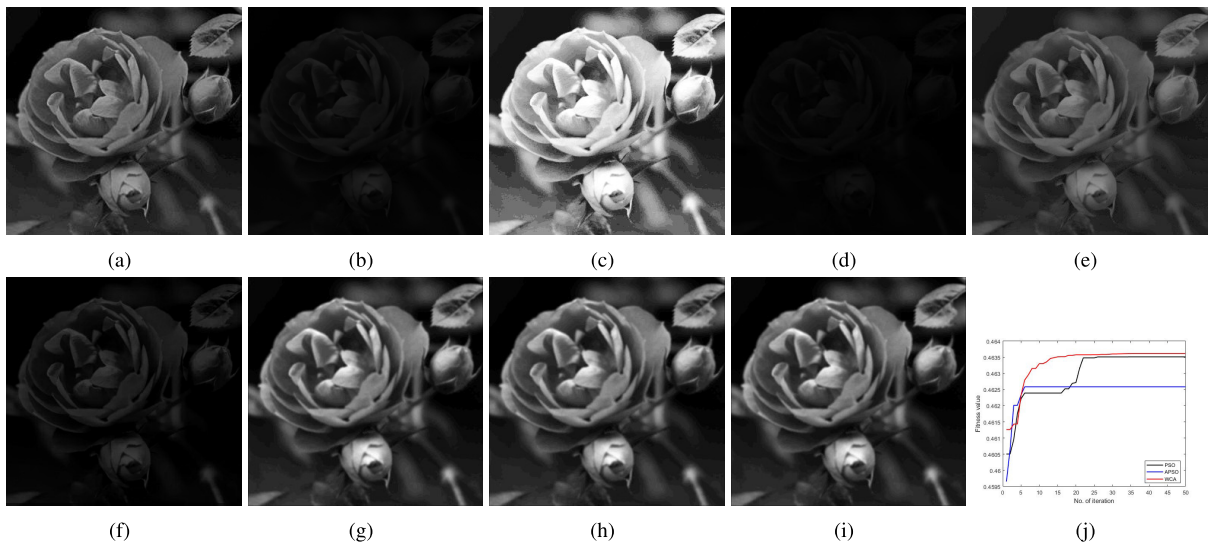


FIGURE 15. Flower images (a) Reference image (b) Test Image (c) HE (d) LCS (e) CLAHE (f) LCM-CLAHE (g) PSO (h) APSO (i) WCA (j) Fitness plot.

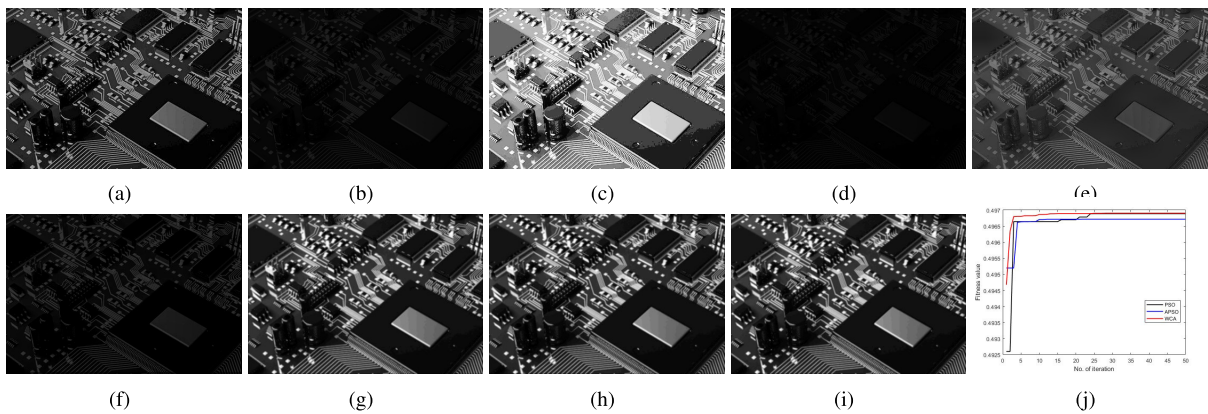


FIGURE 16. Flower images (a) Reference image (b) Test Image (c) HE (d) LCS (e) CLAHE (f) LCM-CLAHE (g) PSO (h) APSO (i) WCA (j) Fitness plot.

for all, except the ‘Car’, and ‘Circuit’ test images. With regard to the AMBE evaluation metric, the method again presented

a better efficiency than PSO and APSO for all test images except ‘Clock’, and ‘Circuit’.

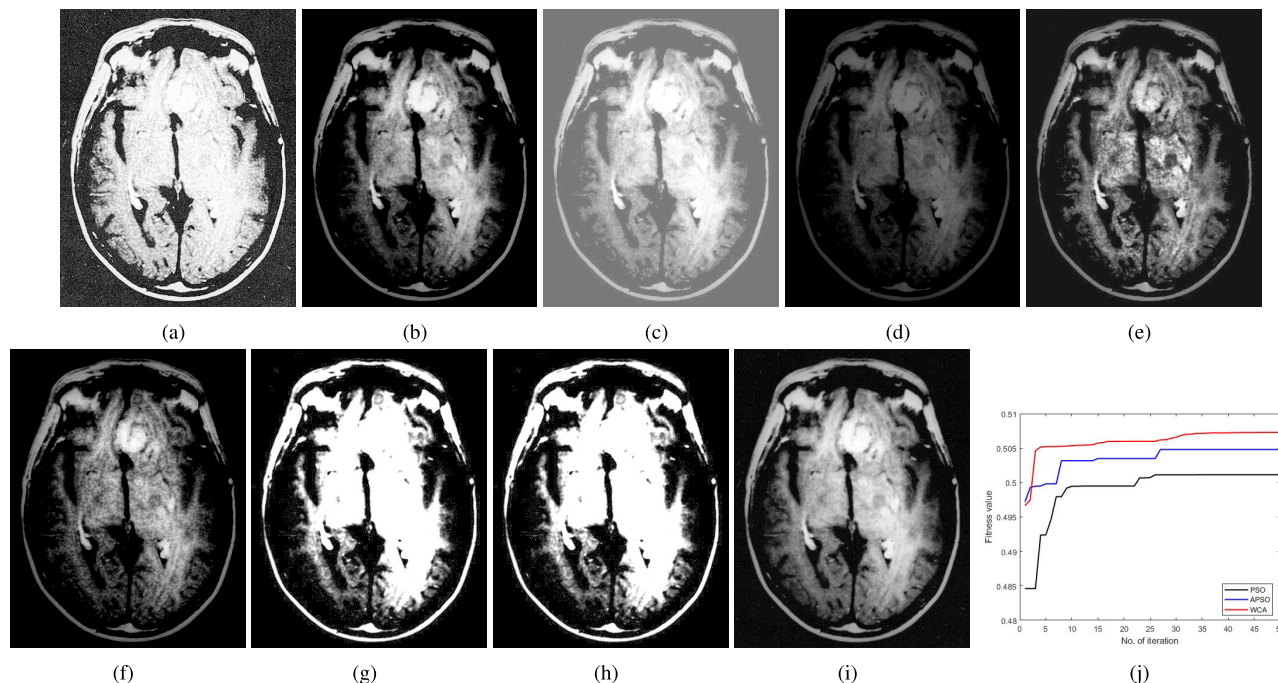


FIGURE 17. Medical images (a) Reference image (b) Test Image (c) HE (d) LCS (e) CLAHE (f) LCM-CLAHE (g) PSO (h) APSO (i) WCA (j) Fitness plot.

As it can also be seen in Tables (4) and (5), the proposed method was found to be more effective in connection to MS-SSIM, IW-SSIM, IW-MSE, IW-PSNR, and FSIM metrics compared to PSO and APSO for all test images except for ‘Indoor’, which was found to be as good as the mentioned methods. The proposed WCA-based method generally showed a performance better than PSO and APSO in all metrics for almost all test images.

1) OPTIMIZATION PERFORMANCE COMPARISON

The various qualities obtained from the enhanced test images performed by different methods are presented in Tables 2, 3, and 4. As it can clearly be seen in the Tables, the NIA-based method produced a better result compared to HE, LCS, CLAHE, and LCM-CLAHE in terms of the objective function fitness result. Whereas the proposed WCA-based method enhanced all the test images with better quality compared to the PSO and APSO methods. Besides, this WCA-based method was found to have a relatively more stability and faster convergence time to the optimal solution than the PSO and APSO techniques, as shown from the fitness plot of corresponding Figures 7-17.

D. RUNNING TIME COMPARISON

The running time of each approach was shown in Table 6. As shown in the Table, the proposed method had a considerable running time compared to the other six techniques. The proposed method required an even longer running time than the PSO and APSO to enhance the images. Because of the two converging criteria, the raining and evaporation processes, the

suggested method requires a longer computational time. PSO and APSO, on the other hand, have only one convergence criterion and so require less computational time than the suggested WCA-based technique. The additional converging criteria, and hence the computing time, are the cost of great optimization ability.

E. LIMITATIONS OF THE STUDY

In this subsection, I wish to highlight several restrictions on this research endeavor. The enhancement of dark gray-scale images was the exclusive subject of this work. Other forms of gray-scale imagery and color image enhancement were excluded. This study also solely examined the traditional WCA image-enhancing capabilities. Hence, the updated WCAs, including the evaporation rate WCA (ErWCA) and other altered variations of it, had not been part of the investigation. The present study compared the image enhancement efficacy of WCA-based methods with the capabilities of HE, LCS, CLAHE, LCM-CLAH, PSO, and APSO. This study was also not based on log and power image transformation, as it focused only on linear transformation due to its simplicity and linearity characteristics. The aforementioned points were identified as limitations of this study. Therefore, herein, the conclusion drawn on the effectiveness of the proposed method is based on the comparison of the dark image enhancement efficiency with the aforementioned techniques.

IV. CONCLUSION

In this paper, the WCA-based image enhancement technique was proposed for a gray-scale dark image enhancement

purposes and compared with other techniques. During the course of this investigation, image enhancement was done in a novel way by combining the intensity transformation and fitness function with WCA.

The image improvement performance of one technique and the quality of the produced image are primarily evaluated using perceptual quality metrics, as the HVS is the ultimate user of the output. In line with this fact, the suggested WCA-based technique outperformed others in terms of FR-IQA metrics MS-SSIM, IW-SSIM, IW-MSE, and IW-PSNR. The proposed technique was also found to have better performance than all other techniques except the HE and CLAHE methods with respect to SSIM and FSIM. The proposed method even showed a performance that exceeded those methods in most images in those metrics. However, it performed less than HE and its variant methods in terms of VIF and IFC. More interestingly, the proposed method was found to be relatively more stable with a faster convergence time than PSO and APSO techniques. Hence, the better performance, in enhancing darker gray-scale images, of the proposed method would make it more applicable to gray-scale images such as medical images, CCTV security images, car plate numbers, and night vision images. Finally, this paper recommended further analysis of the proposed WCA-based method to address the limitations, including the long computational time requirement and those mentioned above.

REFERENCES

- [1] D. Vijayalakshmi, M. K. Nath, and O. P. Acharya, "A comprehensive survey on image contrast enhancement techniques in spatial domain," *Sens. Imag.*, vol. 21, no. 1, pp. 1–40, Dec. 2020.
- [2] Z. Huang, Z. Wang, J. Zhang, Q. Li, and Y. Shi, "Image enhancement with the preservation of brightness and structures by employing contrast limited dynamic quadri-histogram equalization," *Optik*, vol. 226, Jan. 2021, Art. no. 165877.
- [3] A. N. Ismael, M. A. Abd, and H. A. Abd, "Nature inspired algorithms multi-objective histogram equalization for grey image enhancement," *Adv. Comput., Signals Syst.*, vol. 4, no. 1, pp. 36–46, 2020.
- [4] P. Janani, J. Premaladha, and K. S. Ravichandran, "Image enhancement techniques: A study," *Indian J. Sci. Technol.*, vol. 8, no. 22, pp. 1–12, Sep. 2015.
- [5] K. N. Shukla, A. Potnis, and P. Dwivedy, "A review on image enhancement techniques," *Int. J. Eng. Appl. Comput. Sci.*, vol. 2, no. 7, pp. 232–235, 2017.
- [6] R. D. Putra, T. W. Purboyo, and L. Prasasti, "A review of image enhancement methods," *Int. J. Appl. Eng. Res.*, vol. 12, no. 23, pp. 13596–13603, 2017.
- [7] S. Dhariwal, "Comparative analysis of various image enhancement techniques," *Int. J. Electron. Commun. Technol.*, vol. 2, no. 3, pp. 91–95, Sep. 2011.
- [8] G. Li, Y. Yang, X. Qu, D. Cao, and K. Li, "A deep learning based image enhancement approach for autonomous driving at night," *Knowl.-Based Syst.*, vol. 213, Feb. 2021, Art. no. 106617.
- [9] Y. Lee, J. Jeon, Y. Ko, B. Jeon, and M. Jeon, "Task-driven deep image enhancement network for autonomous driving in bad weather," in *Proc. IEEE Int. Conf. Robot. Autom. (ICRA)*, May 2021, pp. 13746–13753.
- [10] L. H. Pham, D. N. Tran, and J. W. Jeon, "Low-light image enhancement for autonomous driving systems using DriveRetinex-Net," in *Proc. IEEE Int. Conf. Consum. Electron.-Asia (ICCE-Asia)*, Nov. 2020, pp. 1–5.
- [11] D. C. Prakash, R. Narayanan, N. Ganesh, M. Ramachandran, S. Chinnasami, and R. Rajeshwari, "A study on image processing with data analysis," *AIP Conf. Proc.*, vol. 2393, no. 1, 2022, Art. no. 020225.
- [12] J. Li, X. Feng, and Z. Hua, "Low-light image enhancement via progressive-recursive network," *IEEE Trans. Circuits Syst. Video Technol.*, vol. 31, no. 11, pp. 4227–4240, Nov. 2021.
- [13] Y.-H. Huang and H. H. Chen, "Deep face recognition for dim images," *Pattern Recognit.*, vol. 126, Jun. 2022, Art. no. 108580.
- [14] A. Vishe, A. Shirsath, S. Gujar, and N. Thakur, "Student attendance system using face recognition," *Engpaper J.*, to be published.
- [15] M. O. Oloyede, G. P. Hancke, and H. C. Myburgh, "Improving face recognition systems using a new image enhancement technique, hybrid features and the convolutional neural network," *IEEE Access*, vol. 6, pp. 75181–75191, 2018.
- [16] J.-W. Wang, N. T. Le, J.-S. Lee, and C.-C. Wang, "Color face image enhancement using adaptive singular value decomposition in Fourier domain for face recognition," *Pattern Recognit.*, vol. 57, pp. 31–49, Sep. 2016.
- [17] J. Ślędzowski, P. Terefenko, A. Giza, P. Forczmański, A. Łysko, W. Maćków, G. Stępień, A. Tomczak, and A. Kurylczyk, "Application of unmanned aerial vehicles and image processing techniques in monitoring underwater coastal protection measures," *Remote Sens.*, vol. 14, no. 3, p. 458, Jan. 2022.
- [18] S. Liu, P. Chen, and M. Woźniak, "Image enhancement-based detection with small infrared targets," *Remote Sens.*, vol. 14, no. 13, p. 3232, Jul. 2022.
- [19] R. Szeliski, *Computer Vision: Algorithms and Applications*. Berlin, Germany: Springer Nature, 2022.
- [20] A. Webb, *Introduction to Biomedical Imaging*. Hoboken, NJ, USA: Wiley, 2022.
- [21] L. Chandrashekar and A. Sreedevi, "A multi-objective enhancement technique for poor contrast magnetic resonance images of brain glioblastomas," *Proc. Comput. Sci.*, vol. 171, pp. 1770–1779, Jan. 2020.
- [22] G. Gao, S. Tong, Z. Xia, B. Wu, L. Xu, and Z. Zhao, "Reversible data hiding with automatic contrast enhancement for medical images," *Signal Process.*, vol. 178, Jan. 2021, Art. no. 107817.
- [23] Y. Zhou, C. Shi, B. Lai, and G. Jimenez, "Contrast enhancement of medical images using a new version of the world cup optimization algorithm," *Quant. Imag. Med. Surg.*, vol. 9, no. 9, pp. 1528–1547, Sep. 2019.
- [24] A. M. Pour, H. Seyedarabi, S. H. A. Jahromi, and A. Javadzadeh, "Automatic detection and monitoring of diabetic retinopathy using efficient convolutional neural networks and contrast limited adaptive histogram equalization," *IEEE Access*, vol. 8, pp. 136668–136673, 2020.
- [25] P. Singh, R. Mukundan, and R. D. Ryke, "Feature enhancement in medical ultrasound videos using contrast-limited adaptive histogram equalization," *J. Digit. Imag.*, vol. 33, no. 1, pp. 273–285, Feb. 2020.
- [26] M. S. Ahmed, T. T. Aurpa, and M. A. K. Azad, "Fish disease detection using image based machine learning technique in aquaculture," *J. King Saud Univ. Comput. Inf. Sci.*, vol. 34, no. 8, pp. 5170–5182, Sep. 2022.
- [27] G. U. Nneji, J. Cai, J. Deng, H. N. Monday, E. C. James, and C. C. Ukwuoma, "Multi-channel based image processing scheme for pneumonia identification," *Diagnostics*, vol. 12, no. 2, p. 325, Jan. 2022.
- [28] U. Shafi, R. Mumtaz, Z. Shafaq, S. M. H. Zaidi, M. O. Kaifi, Z. Mahmood, and S. A. R. Zaidi, "Wheat rust disease detection techniques: A technical perspective," *J. Plant Diseases Protection*, vol. 129, pp. 489–504, Jan. 2022.
- [29] N. Kheradmandi and V. Mehranfar, "A critical review and comparative study on image segmentation-based techniques for pavement crack detection," *Construct. Building Mater.*, vol. 321, Feb. 2022, Art. no. 126162.
- [30] N. Safaei, O. Smadi, A. Masoud, and B. Safaei, "An automatic image processing algorithm based on crack pixel density for pavement crack detection and classification," *Int. J. Pavement Res. Technol.*, vol. 15, no. 1, pp. 159–172, Jan. 2022.
- [31] P. Patel and A. Bhandari, "A review on image contrast enhancement techniques," *Int. J. Online Sci.*, vol. 5, no. 5, pp. 14–18, 2019.
- [32] M. Kaushal, B. S. Khehra, and A. Sharma, "Water cycle algorithm based multi-objective contrast enhancement approach," *Optik*, vol. 140, pp. 762–775, Jul. 2017.
- [33] W. Wang, X. Wu, X. Yuan, and Z. Gao, "An experiment-based review of low-light image enhancement methods," *IEEE Access*, vol. 8, pp. 87884–87917, 2020.
- [34] L. Chandrashekar and A. Sreedevi, "A nature inspired algorithm for enhancement of fused MRI and CT brain images," in *Emerging Research in Computing, Information, Communication and Applications*. Cham, Switzerland: Springer, 2022, pp. 11–24.

- [35] S. K. Suguna, R. Ranganathan, J. Sangeetha, S. Shandilya, and S. K. Shandilya, "Application of nature—Inspired algorithms in medical image processing," in *Advances in Nature-Inspired Computing and Applications*. Cham, Switzerland: Springer, 2019, pp. 61–100.
- [36] N. Dey, *Applications of Firefly Algorithm and Its Variants*. Cham, Switzerland: Springer, 2020.
- [37] C. Ding, X. Pan, X. Gao, L. Ning, and Z. Wu, "Three adaptive sub-histograms equalization algorithm for maritime image enhancement," *IEEE Access*, vol. 8, pp. 147983–147994, 2020.
- [38] K. G. Dhal and S. Das, "Chaotic differential-evolution-based fuzzy contrast stretching method," in *Applied Metaheuristic Computing*. Hershey, PA, USA: IGI Global, 2018, pp. 71–94.
- [39] S. Samanta, A. Mukherjee, A. S. Ashour, N. Dey, J. M. R. S. Tavares, W. B. A. Karãa, R. Taiar, A. T. Azar, and A. E. Hassanien, "Log transform based optimal image enhancement using firefly algorithm for autonomous mini unmanned aerial vehicle: An application of aerial photography," *Int. J. Image Graph.*, vol. 18, no. 4, Oct. 2018, Art. no. 1850019.
- [40] A. S. Ashour, S. Samanta, N. Dey, N. Kausar, W. B. Abdessalemkaraa, and A. E. Hassanien, "Computed tomography image enhancement using cuckoo search: A log transform based approach," *J. Signal Inf. Process.*, vol. 6, no. 3, pp. 244–257, 2015.
- [41] S.-I. Bejinariu, H. Costin, F. Rotaru, R. Luca, C. Nita, and D. Costin, "Image enhancement by multiobjective optimization and bio-inspired heuristics," in *Proc. E-Health Bioeng. Conf. (EHB)*, Jun. 2017, pp. 442–445.
- [42] A. Gorai and A. Ghosh, "Gray-level image enhancement by particle swarm optimization," in *Proc. World Congr. Nature Biologically Inspired Comput. (NaBIC)*, 2009, pp. 72–77.
- [43] K. S. Song and M. G. Kang, "Optimized tone mapping function for contrast enhancement considering human visual perception system," *IEEE Trans. Circuits Syst. Video Technol.*, vol. 29, no. 11, pp. 3199–3210, Nov. 2019.
- [44] K. G. Dhal and S. Das, "Cuckoo search with search strategies and proper objective function for brightness preserving image enhancement," *Pattern Recognit. Image Anal.*, vol. 27, no. 4, pp. 695–712, Oct. 2017.
- [45] A. K. Randhawa and A. Bamotra, "Review paper on image enhancement and its techniques," *Int. J. Eng. Comput. Sci.*, pp. 21443–21447, Jun. 2017.
- [46] Y. Chang, C. Jung, P. Ke, H. Song, and J. Hwang, "Automatic contrast-limited adaptive histogram equalization with dual gamma correction," *IEEE Access*, vol. 6, pp. 11782–11792, 2018.
- [47] S. Gupta and Y. Kaur, "Review of different local and global contrast enhancement techniques for a digital image," *Int. J. Comput. Appl.*, vol. 100, no. 18, pp. 18–23, Aug. 2014.
- [48] J. Ma, X. Fan, S. X. Yang, X. Zhang, and X. Zhu, "Contrast limited adaptive histogram equalization-based fusion in YIQ and HSI color spaces for underwater image enhancement," *Int. J. Pattern Recognit. Artif. Intell.*, vol. 32, no. 7, Jul. 2018, Art. no. 1854018.
- [49] M. S. Hitam, E. A. Awalludin, W. N. Jawahir Hj Wan Yussof, and Z. Bachok, "Mixture contrast limited adaptive histogram equalization for underwater image enhancement," in *Proc. Int. Conf. Comput. Appl. Technol. (ICCAT)*, Jan. 2013, pp. 1–5.
- [50] G. Singh and A. Mittal, "Various image enhancement techniques—A critical review," *Int. J. Innov. Sci. Res.*, vol. 10, no. 2, pp. 267–274, 2013.
- [51] S. Mohan and M. Ravishankar, "Modified contrast limited adaptive histogram equalization based on local contrast enhancement for mammogram images," in *Proc. Int. Conf. Adv. Inf. Technol. Mobile Commun. (AIM/CCPE)*, Bengaluru, India, Apr. 2012, pp. 397–403.
- [52] G. F. C. Campos, S. M. Mastelini, G. J. Aguiar, R. G. Mantovani, L. F. D. Melo, and S. Barbon, "Machine learning hyperparameter selection for contrast limited adaptive histogram equalization," *EURASIP J. Image Video Process.*, vol. 2019, no. 1, pp. 1–18, Dec. 2019.
- [53] V. Stimper, S. Bauer, R. Ernstorfer, B. Schölkopf, and R. P. Xian, "Multidimensional contrast limited adaptive histogram equalization," *IEEE Access*, vol. 7, pp. 165437–165447, 2019.
- [54] J. Hemanth and V. E. Balas, *Nature Inspired Optimization Techniques for Image Processing Applications*. Cham, Switzerland: Springer, 2019.
- [55] S. R. J. Ramson, K. L. Raju, S. Vishnu, and T. Anagnostopoulos, "Nature inspired optimization techniques for image processing—A short review," in *Nature Inspired Optimization Techniques for Image Processing Applications*. Springer, 2019, pp. 113–145.
- [56] K. G. Dhal, S. Ray, A. Das, and S. Das, "A survey on nature-inspired optimization algorithms and their application in image enhancement domain," *Arch. Comput. Methods Eng.*, vol. 26, no. 5, pp. 1607–1638, Nov. 2019.
- [57] K. Dhruve and D. Kaur, "Nature-inspired algorithms for image enhancement," in *Proc. IEEE Int. Midwest Symp. Circuits Syst. (MWSCAS)*, Aug. 2021, pp. 101–104.
- [58] S. Ghosh, S. Roy, U. Kumar, and A. Mallick, "Gray level image enhancement using cuckoo search algorithm," in *Advances in Signal Processing and Intelligent Recognition Systems*. Cham, Switzerland: Springer, 2014, pp. 275–286.
- [59] K. G. Dhal, M. I. Quraishi, and S. Das, "Performance analysis of chaotic lévy bat algorithm and chaotic cuckoo search algorithm for gray level image enhancement," in *Information Systems Design and Intelligent Applications*. Cham, Switzerland: Springer, 2015, pp. 233–244.
- [60] A. K. Bhandari and S. Maurya, "Cuckoo search algorithm-based brightness preserving histogram scheme for low-contrast image enhancement," *Soft Comput.*, vol. 24, no. 3, pp. 1619–1645, Feb. 2020.
- [61] K. G. Dhal and S. Das, "A dynamically adapted and weighted bat algorithm in image enhancement domain," *Evolving Syst.*, vol. 10, no. 2, pp. 129–147, Jun. 2019.
- [62] S.-I. Bejinariu, H. Costin, F. Rotaru, and R. Luca, "Image enhancement using chaotic maps and bio-inspired multi-objective optimization," in *Proc. Int. Symp. Signals, Circuits Syst. (ISSCS)*, Jul. 2019, pp. 1–4.
- [63] H. Eskandar, A. Sadollah, A. Bahreinejad, and M. Hamdi, "Water cycle algorithm—A novel metaheuristic optimization method for solving constrained engineering optimization problems," *Comput. Struct.*, vols. 110–111, pp. 151–166, Nov. 2012.
- [64] X.-S. Yang, "Cuckoo search and firefly algorithm: Overview and analysis," in *Cuckoo Search and Firefly Algorithm*. 2014, pp. 1–26.
- [65] M. Elloumi, R. Kallel, and G. Boukettaya, "A comparative study of GA and APSO algorithm for an optimal design of a standalone PV/battery system," in *Proc. 15th Int. Multi-Conf. Syst., Signals Devices (SSD)*. IEEE, 2018, pp. 1104–1109.
- [66] A. H. Gandomi, G. J. Yun, X.-S. Yang, and S. Talatahari, "Chaos-enhanced accelerated particle swarm optimization," *Commun. Nonlinear Sci. Numer. Simul.*, vol. 18, no. 2, pp. 327–340, 2013.
- [67] A. Sadollah, H. Eskandar, and J. H. Kim, "Water cycle algorithm for solving constrained multi-objective optimization problems," *Appl. Soft Comput.*, vol. 27, pp. 279–298, Feb. 2015.
- [68] M. Nasir, A. Sadollah, Y. H. Choi, and J. H. Kim, "A comprehensive review on water cycle algorithm and its applications," *Neural Comput. Appl.*, vol. 32, no. 23, pp. 17433–17488, Dec. 2020.
- [69] H. Eskandar, A. Sadollah, and A. Bahreinejad, "Weight optimization of truss structures using water cycle algorithm," *Iran Univ. Sci. Technol.*, vol. 3, no. 1, pp. 115–129, 2013.
- [70] A. Sadollah, H. Eskandar, H. M. Lee, D. G. Yoo, and J. H. Kim, "Water cycle algorithm: A detailed standard code," *SoftwareX*, vol. 5, pp. 37–43, Jan. 2016.
- [71] S. Idrani and S. Jain, "Edge detection of license plate using Sobel operator," in *Proc. Int. Conf. Electr., Electron., Optim. Techn. (ICEEOT)*, Mar. 2016, pp. 3561–3563.
- [72] G. N. Chaple, R. D. Daruwala, and M. S. Gofane, "Comparisons of Robert, Prewitt, Sobel operator based edge detection methods for real time uses on FPGA," in *Proc. Int. Conf. Technol. Sustain. Develop. (ICTSD)*, Feb. 2015, pp. 1–4.
- [73] O. Vincent and O. Folorunso, "A descriptive algorithm for Sobel image edge detection," in *Proc. InSITE Conf.*, 2009, pp. 97–107.
- [74] B. Subramani and M. Veluchamy, "Fuzzy gray level difference histogram equalization for medical image enhancement," *J. Med. Syst.*, vol. 44, no. 6, pp. 1–10, Jun. 2020.
- [75] K. Gopal Dhal, I. Quraishi, and S. Das, "A chaotic lévy flight approach in bat and firefly algorithm for gray level image enhancement," *Int. J. Image, Graph. Signal Process.*, vol. 7, no. 7, pp. 69–76, Jun. 2015.
- [76] T. Laksmi, T. Madhu, K. Kavya, and S. E. Basha, "Novel image enhancement technique using CLAHE and wavelet transforms," *Int. J. Sci. Eng. Technol.*, vol. 5, no. 11, pp. 507–511, 2016.

- [77] Z. Ye, M. Wang, Z. Hu, and W. Liu, "An adaptive image enhancement technique by combining cuckoo search and particle swarm optimization algorithm," *Comput. Intell. Neurosci.*, vol. 2015, Feb. 2015, Art. no. 825398.
- [78] R. Dosselmann and X. D. Yang, "A comprehensive assessment of the structural similarity index," *Signal, Image Video Process.*, vol. 5, no. 1, pp. 81–91, Mar. 2011.
- [79] U. Sara, M. Akter, and M. S. Uddin, "Image quality assessment through FSIM, SSIM, MSE and PSNR—A comparative study," *J. Comput. Commun.*, vol. 7, no. 3, pp. 8–18, 2019.
- [80] A. Gore and S. Gupta, "Full reference image quality metrics for JPEG compressed images," *AEU Int. J. Electron. Commun.*, vol. 69, no. 2, pp. 604–608, Feb. 2015.
- [81] Y. Qi, Z. Yang, W. Sun, M. Lou, J. Lian, W. Zhao, X. Deng, and Y. Ma, "A comprehensive overview of image enhancement techniques," *Arch. Comput. Methods Eng.*, vol. 29, pp. 583–607, Apr. 2022.
- [82] X. Zhang, X. Feng, W. Wang, and W. Xue, "Edge strength similarity for image quality assessment," *IEEE Signal Process. Lett.*, vol. 20, no. 4, pp. 319–322, Apr. 2013.
- [83] T. Samajdar and M. I. Quraishi, "Analysis and evaluation of image quality metrics," in *Proc. 2nd Int. Conf. INDIA*, vol. 2, 2015, pp. 369–378.
- [84] L. Zhang, L. Zhang, X. Mou, and D. Zhang, "FSIM: A feature similarity index for image quality assessment," *IEEE Trans. Image Process.*, vol. 20, no. 8, pp. 2378–2386, Aug. 2011.
- [85] K. Joy and E. G. Sarma, "Recent developments in image quality assessment algorithms: A review," *J. Theor. Appl. Inf. Technol.*, vol. 65, no. 1, pp. 192–201, 2014.
- [86] Z. Wang and Q. Li, "Information content weighting for perceptual image quality assessment," *IEEE Trans. Image Process.*, vol. 20, no. 5, pp. 1185–1198, May 2011.
- [87] H. R. Sheikh, A. C. Bovik, and G. de Veciana, "An information fidelity criterion for image quality assessment using natural scene statistics," *IEEE Trans. Image Process.*, vol. 14, no. 12, pp. 2117–2128, Dec. 2005.
- [88] H. R. Sheikh and A. C. Bovik, "Image information and visual quality," *IEEE Trans. Image Process.*, vol. 15, no. 2, pp. 430–444, Feb. 2006.



EYOB MERSHA WOLDAMANUEL received the B.Sc. degree in electrical and computer engineering from Haramaya University, Ethiopia, in 2014, and the M.Sc. degree in electronics and communication engineering from Adama Science and Technology University (ASTU), Ethiopia, in 2019.

He was an Assistant Lecturer with the Haramaya Institute of Technology, Haramaya University, from 2015 to 2017. Since September 2019, he has been a Lecturer and a Researcher with the School of Electrical and Computer Engineering, Haramaya Institute of Technology, Haramaya University. He is the author of the article titled *Enhanced Adaptive Code Modulation for Rainfall Mitigation in Ethiopia* (Springer, 2022). His current research interests include applied soft computing, the application of AI for communication systems, massive-MIMO, mmWave and sub-THz communication channel modeling, and microwave and satellite communication.

• • •